Science
AAAS

Supplementary Materials for

Oncometabolite D-2HG alters T cell metabolism to impair $CD8^+$ T cell function

Giulia Notarangelo *et al*.

Corresponding author: Marcia C. Haigis, Marcia_haigis@hms.harvard.edu

Science **377**, 1519 (2022)
DOI: 10.1126/science.abj5104

The PDF file includes:

Other Supplementary Material for this manuscript includes the following:

Materials and Methods:

Cell lines

The mouse glioma 261 (GL-261) cell line was purchased from NCI-Frederick Cancer Research Tumor Repository and cultured in RPMI-1640 medium (Gibco, 11875119). Platinum-E cells (Cell Biolabs, RV-101) were cultured in DMEM (Gibco, 11995073) and were selected in 1 μg/mL puromycin (InvivoGen, ant-pr-1) and 10 μg/mL blasticidin (Sigma, 15205-25MG). B16-OVA cell lines were generated as previously described [53] and cultured in RPMI-1640 medium. MC38 cells were cultured in DMEM medium. B16 cells were cultured in RPMI-1640 medium. All media were supplemented with 10% FBS and 1% penicillin-streptomycin (Thermo Fisher Scientific, 15140122).

Mice

Wild type C57BL/6 were purchased from the Jackson Laboratory (000664). OT-1 (C57BL/6-tg(tcra/tcrb)1100Mjb/J) mice were purchased from the Jackson Laboratory (003831) and bred in-house. 7–10-week-old female mice were used for all experiments. All experimental mice were housed in pathogen-free conditions and were handled in accordance with animal care guidelines from the Harvard Medical School Standing Committee on Animals and the National Institutes of Health.

Overexpression by lentiviral transduction in MC38 and B16

Human IDH1 WT and R132H cDNAs were cloned into pLenti-EFIa-IRES-Hygro (plasmids were a gift from Sam McBrayer, UT Southwestern). Lentivirus was made by Turbofect-based transfection (Thermo Fisher Scientific, R0533) of HEK293T using lentiviral packaging plasmids. Supernatant was replaced after 24 hours, and viral supernatant was collected after 48 and 72 hours and filtered through a 45-μm filter. Undiluted viral supernatant was supplemented by polybrene (Sigma, TR-1003-G) at a final concentration of 8 μg/mL and applied to previously seeded MC38 or B16 cell lines for 24 hours. Lentivirally infected cell lines were selected in cultured medium containing hygromycin (700 μg/mL for B16 and 300 μg/mL for MC38).

Syngeneic mouse tumor models and TIL and TIF isolation

At 8-10 weeks, female C57BL/6 were anesthetized with isoflurane, shaved at the injection site, and subcutaneously injected in the abdominal flank with 250,000 MC38 or B16 cells. Tumors were monitored every 2-3 days. On day 16, mice were sacrificed for tissue harvest. Tumor intestinal fluid (TIF) was harvested by centrifugation at 400 g for 15 minutes using a 20 μM nylon net filter (EMD Millipore, NY2004700). Tumors were digested in 1x DPBS, containing calcium and magnesium, and 250 units/mL of Type I Collagenase (Worthington Biochemical Corporation, LS004194). Samples were then dissociated using GentleMACS (Miltenyl, 130-093-235), incubated for 20 minutes at 37°C with gentle rocking, further dissociated by GentleMACS, and then filtered through a 70 μM filter. TILs were subsequentially enriched by centrifugation through a 40%/70% Percoll gradient at 800 g for 20 minutes with the acceleration and brakes off. Leukocytes were recovered from the interface.

Chemicals

D-2HG (11605), L-2HG (11876), Rotenone (83-79-4), and GSK2837808A (1445879-21-9) were purchased from Cayman Chemicals. Nicotinamide mononucleotide (N3501-25MG), N-Acetyl-L-

cysteine (A7250-5G), Hydrogen peroxide solution (H1009-5ML), O-(Carboxymethyl)hydroxylamine hemihydrochloride (AOA, C13408-1G), Sodium oxamate (O2751-5G), Antimycin A (A8674-50MG), and Oligomycin A (O4876-5MG) were purchased from Sigma. FCCP (103015-100) was purchased from Agilent. U-$^{13}C_6$ D-Glucose (CLM-1396-0.5) was purchased from Cambridge Isotope Laboratories. U-$^{13}C_5$ D-2HG and L-2HG were generously provided by Agios Pharmaceuticals.

2HG uptake and quantification of intracellular concentration

Activated $CD8^+$ T cells were cultured for 24 hours in a range of D- or L-2HG concentrations. Cells were pelleted and the media was removed following careful centrifugation at 13,000 rpm for 20 seconds using a microcentrifuge. Following the same procedure, 3 washes with ice-cold PBS were performed to ensure that all 2HG-containing media was removed. Intracellular metabolites were subsequently extracted in 80% MeOH. Samples were analyzed by mass spectrometry as described below. 2HG content (mol) inside the samples was determined by interpolation using 2HG total ion counts measured in the standards. 2HG content was then divided by cell number to obtain the amount per cell (mol/cell). Finally, to obtain the intracellular concentration of 2HG inside an activated $CD8^+$ T cell, 2HG content expressed as mol/cell was divided by the estimated volume of an activated murine $CD8^+$ T cell, which is close to 500 femtoliters, as reported in the literature [17].

Isolation and activation of naïve $CD8^+$ T lymphocytes

Naïve $CD8^+$ T lymphocytes were isolated from mouse spleens by negative selection using the Naïve $CD8a^+$ T cell Isolation Kit from Miltenyi Biotec (130-096-543). Following isolation, naïve $CD8^+$ T lymphocytes were activated with plate-bound 4 μg/mL αCD3 (BioXCell, BE0001-1) and 4 μg/mL αCD28 (BioXCell, BE0015-1) and cultured in RPMI-1640 supplemented with 10% heat-inactivated FBS, 10 mM HEPES (Gibco, 15630080), 0.05 mM 2-mercaptoethanol (Sigma, M3148-100ML), and 1% penicillin-streptomycin. After 48 hours, the media was refreshed and 100 U/mL recombinant murine IL-2 (PeproTech, 212-12-20) were added. For intracellular cytokine staining, $CD8^+$ T cells were stimulated with 100 ng/mL PMA (Sigma, P1585-1MG) and 500 ng/mL ionomycin (Sigma, I0634-1MG) in the presence Brefeldin A (BD Biosciences, 555029) for 4 hours.

Degranulation assay

Naïve $CD8^+$ T cells were activated in plates coated with αCD3 and αCD28 and cultured for 6 days in the presence of IL-2, refreshing the media every 3 days. On day 6, activated $CD8^+$ T cells were restimulated with 5 μg/mL αCD3 in the presence of αCD107a-PE (clone 1D4B, Biolegend), αCD107b-PE (clone M3/84, Biolegend) and Brefeldin A. αCD28 stimulation was used as a negative control. After 5-6 hours, cells were washed and immediately analyzed via flow cytometry. The percentage of PE-positive cells indicates cells that have degranulated.

In vitro killing assay

Naïve $CD8^+$ OT-1 T cells were activated for 72 hours in plates coated with 1 μg/mL αCD3 and 1 μg/mL αCD28 in the presence of 100 U/mL IL-2 and 10 ng/mL IL-12 (PeproTech, 210-12-50). After 72 hours, 5,000 activated $CD8^+$ OT-1 T cells and 30,000 OVA^{wt} or $OVA^{\Delta 257\text{-}264}$-expressing GFP^+B16 cancer cells were plated together in a 96-well plate. After 24 hours, plates were

trypsinized, resuspended in MACS buffer (1X PBS, 1% FBS, and 2 mmol/L EDTA) and analyzed by flow cytometry.

Overexpression by retroviral transduction in $CD8^+$ T cells

The cDNAs of D-2HGDH and bacterial cyto*Lb*NOX were cloned into pMSCV PIG (Addgene, 21654) using MIuI and BamHI restriction sites. Recombinant retrovirus was made by co-transfection of pMSCV PIG and pCL-Eco (Addgene, 12371) into Platinum-E cells using TurboFect transfection reagent. Viral supernatants were collected 48 and 72 hours after transfection and cellular debris was removed by filtrating the supernatants through 45-μm filters (Thermo Fisher Scientific, 723-9945). Naïve $CD8^+$ T lymphocytes were stimulated for 24 hours with plate-bound 1 μg/mL αCD3 and 1 μg/mL αCD28 and cultured in complete RPMI supplement with 100 μM non-essential amino acids (Gibco, 11140050), 1 mM sodium pyruvate (Gibco, 11360-070) and 100 U/mL recombinant IL-2. After 24 hours, T cells were spinfected at 37°C and 1900 rpm for 90 minutes with freshly collected, undiluted retrovirus containing 10 μg/mL polybrene. 4 hours post-spinfection, the viral media was removed and fresh complete RPMI media was added. A second round of transduction was performed the next day, and the media was once again refreshed 4 hours after spinfection. GFP^+ transduced T cells were selected by flow-cytometry sorting using a 70-μm nozzle.

Seahorse assays

The Agilent Seahorse XF Real-Time ATP Rate Assay Kit (Agilent, 103592–100) was used to detect the ATP production rates of mitochondrial oxidative phosphorylation and glycolysis, respectively. Oxygen consumption rates (OCR), extracellular acidification rates (ECAR) and ATP production rates of mitochondrial oxidative phosphorylation and glycolysis were determined on the XFe96 Extracellular Flux Analyzer (Agilent), according to the manufacturer's instructions and protocols. The day before measurement, the probe plate was hydrated with HPLC grade water in a CO_2-free incubator and the solution was replaced the following day with XF Calibrant and kept in a 37 °C CO_2-free incubator for at least one hour. For all assays, activated $CD8^+$ T cells were pre-treated with drugs for 24 hours. After 24 hours of treatment, activated $CD8^+$ T cells were seeded into poly-L-lysine-coated XF96 cell culture microplates (Agilent, 101085-004) at the density of 60,000 cells/well. Cells were seeded in Seahorse XP RPMI medium (Agilent, 103576-100), containing 5 mM glucose (Sigma, G8270-100G), 2 mM L-glutamine (Thermo Fisher Scientific, 25030081), 1 mM sodium pyruvate, 1% FBS. To measure maximal respiratory capacity, 1.5 μM FCCP was injected from port A.

Mitochondrial membrane potential quantification

$CD8^+$ T cells were seated in a 96 well plate and stained with 200 nM TMRE (Abcam, ab113852) at 37 °C for 30 minutes. As a control, to depolarize the mitochondrial membrane, 20 nM FCCP was added for 10 minutes prior to TMRE staining. To modulate the state of the membrane potential, the following ETC inhibitors were added for 15 minutes prior to TMRE staining: 2 μM rotenone, 1 μM antimycin A, 1 μM oligomycin, and 1.5 μM FCCP. Cells were washed twice with PBS, and immediately analyzed on the LSR II flow cytometer.

Reactive oxygen species quantification

$CD8^+$ T cells were seated in a 96 well plate and stained with 5 μM CellROX Green (Thermo Fisher Scientific, C10444). 10 mM NAC and 100 μM H_2O_2 were included as negative and positive

controls, respectively. Cells were wash twice with PBS, and immediately analyzed on the LSR II flow cytometer.

Western blotting

RIPA buffer containing 150 mM NaCl, 1% NP-40, 0.5% sodium deoxycholate, 0.1% SDS, 25 mM Tris (pH 7.4) and supplemented with protease inhibitors (Roche, 11873580001) and phosphate inhibitors 2/3 (Sigma, P5726 and P0044) was used to prepare lysates. Proteins were denatured at 95°C unless they were used to blot for ETC complexes and were therefore denatured at 50°C. Protein levels were normalized using Pierce BCA protein assay kit (Thermo Fisher Scientific, 23225). Western blotting was performed using the following primary antibodies: ATP5a (Abcam, ab14748), MTCO1 (Novus, RB24524), SDHa (Thermo Fischer Scientific, 459200), UQCRC2 (Proteintech, 14742-1-AP), Tubulin (Cell Signaling, 2144S), VDAC1 (Abcam, ab14734), FLAG (Cell Signaling, 2368S), D-2HGDH (Proteintech, 13895-1-AP), L-2HGDH (Proteintech, 15707-1-AP), and tri-methyl histone H3 antibody sampler kit (Cell Signaling, 9783T).

Mitochondrial DNA quantification

Total DNA was extracted using DNeasy Blood and Tissue Kit (Qiagen, 69506) and analyzed by real time quantitative PCR. Mitochondrial DNA quantification was performed with mitochondrial markers: CO1 (F: TGCTAGCCGCAGGCATTAC, R: GGGTGCCCAAAGAATCAGAAC), ND1 (F: CCGCAAGGGAAAGATGAAAGAC, R: TCGTTTGGTTTCGGGGTTTC), and 16S (F: CCGCAAGGGAAAGATGAAAGAC, R: TCGTTTGGTTTCGGGGTTTC). Mitochondrial DNA was normalized to nuclear DNA marker: NDUFV1 (F: CTTCCCCACTGGCCTCAAG, R: CCAAAACCCAGTGATCCAGC)

Metabolite measurement by mass spectrometry

For steady state metabolomics experiments comparing D- to L-2HG as shown in Fig. 2B, 0.5 million activated $CD8^+$ T cells were cultured for 24 hours in the presence of 20 mM D-2HG, 20 mM L-2HG or left untreated.

For $^{13}C_6$ glucose tracing studies as shown in Figure 2E and supplementary figure 5B, 10 mM $^{13}C_6$ glucose (CLM-1396-1, Cambridge Isotope Laboratories) was provided at the same time as 20 mM D-2HG, 20 mM L-2HG, 20 mM oxamate, or 10 μM GSK2837808A to activated $CD8^+$ T cells and metabolites were analyzed after 24 hours of treatment. For all $^{13}C_6$ tracing studies, RPMI-1640 was replaced by glucose-free RPMI-1640 (Thermo Fischer Scientific, 11879020) and FBS was replaced by dialyzed FBS.

For $^{13}C_6$ glucose tracing studies with antimycin A treatment as shown in Figure 3C, activated $CD8^+$ T cells were pre-treated with 20 mM D-2HG for 2 hours, before 10 mM $^{13}C_6$ glucose was added in the presence or absence of 1 μM antimycin A for an additional 2 hours. D-2HG was kept for the entirety (4 hours) of the assay.

For $^{13}C_5$ 2HG tracing studies as shown in supplementary figure 2E, 20 mM $^{13}C_5$ D-2HG (Agios Pharmaceuticals), or 20 mM $^{13}C_5$ L-2HG (Agios Pharmaceuticals) were provided to activated $CD8^+$ T cells for 2 days.

To harvest samples, cells were transferred to Eppendorf tubes, rapidly pelleted at 4°C (20 seconds, 13,000 rpm), and the supernatants were then transferred to a new tube. Next, pellets were washed twice with ice-cold PBS using the same centrifugation protocol. To extract metabolites from cultured cells, 100 mL 80% MeOH were added to each tube. To extract metabolites from media, 10 mL of media were combined with 90 mL of 80% MeOH. Samples were left on ice for 15

minutes, and vortexed every 5 minutes. Methanol extracts were then centrifuged at 4°C for 10 min at 13,000 rpm and the upper phase containing polar metabolites was collected and dried using a SPD111V Modular Concentrator (Thermo Fisher Scientific). Dried metabolites were stored at -80°C until ready for analysis. Dried metabolites were resuspended in 50% water/50% acetonitrile, and the extract was separated by using an iHILIC column (5μm, 150 × 2.1 mm I.D., HILICON) coupled to a Thermo Fisher Scientific SII UPLC system. The iHILIC column was used with the following buffers and linear gradient: A = water with 20 mM ammonium carbonate with 0.1% ammonium hydroxide, B = acetonitrile. The gradient was run at a flow rate of 0.150 mL/min as follows: 0 – 20 min linear gradient from 80% to 20% B; 20 – 20.5 min linear gradient from 20% to 8-% B; 20.5 – 28 min hold at 80% B; 28 – 30 min hold to waste at 80% B. Mass spectrometry detection was carried out on a Q Extractive HF-X orbitrap mass spectrometer with a HESI source operated in negative mode. Analysis was performed using TraceFinder (Thermo Fisher Scientific) and raw ion counts were normalized based on protein levels. 2HG measurements were sometimes determined using the Agilent 6470 Triple Quadrupole mass spectrometer (Agilent LC-MS). Analytes were eluted in buffer A (97 % H_2O, 3% MeOH, 10 mM Tributylamine, 15 mM Glacial Acetic Acid, pH 5.5) and buffer B (10 mM Tributylamine, 15 mM Glacial Acetic Acid in 100% MeOH), and samples were run on a ZORBAX Extend-C18, 2.1 x 150 mm, 1.8 μm (Agilent). The gradient was run at a flow rate of 0.25 mL/min for 2.5 minutes of buffer A, followed by a linear gradient (100% buffer A to 80% buffer A) for 5 minutes, followed by a linear gradient (80% buffer A to 55% buffer A) for 5.5 minutes, followed by a linear gradient (55% buffer A to 1% buffer A) for 7 minutes, followed by 4 minutes with (1% buffer A). Samples were ionized (with negative polarity) using Agilent Jet Spray ionization.

For TIF analysis, 1 μL of TIF was extracted in 50 μL of 80% MeOH. D-2HG concentrations were determined using an internal standard curve with $^{13}C_5$ D-2HG.

Flow cytometry

Cells were pelleted and washed twice in PBS prior to staining with Fixable Viability Dye (eBioscience, 65-0866-14) or LIVE/DEAD Fixable near-IR dead cell stain kit (Thermo Fisher Scientific, L34976). Surface staining was performed on ice in FACS Buffer (1X PBS, 3% FBS). Cell surface markers used: CD25 (clone PC61) and CD69 (clone H1.2F3), CD45.2 (Clone 104), CD8b (Clone YTS156.7.7), CD3 (Clone 17A2), CD4 (Clone RM4-5), CD11b (Clone M1/70), and CD44 (Clone IM7). Intracellular markers used: Granzyme B (Clone QA18A28), FoxP3 (Clone FJK-16s), Interferon-γ (Clone XMG1.2), and Ki-67 (Clone 16A8). Intracellular granzyme B staining was performed using the FoxP3 fix/perm kit (eBioscience). Intracellular cytokine staining was performed using BD Cytofix/Cytoperm kit (BD Biosciences, BDB554714). All antibodies were purchased from BD Bioscience or Biolegend. Proliferation was assessed by CellTrace Violet staining (Thermo Fisher Scientific, C34571). Division index was calculated from the total number of divisions divided by the number of live cells at the start of culture. Data were analyzed on an LSR II flow cytometer and FlowJo software (TreeStar)

NAD^+/NADH ratio

0.25 million $CD8^+$ T cells were plated in the presence of 20 mM D-2HG, 20 mM L-2HG, 1 mM NMN (positive control), 20 mM oxamate, or 10 μM GSK2837808A for 24 hours. NAD^+/NADH ratio was determined using a commercially available kit (Abcam, ab65348), following the manufacturer's instructions.

ELISA

50,000 naïve $CD8^+$ T cells were plated in triplicates in a 96-well plate coated with 4 μg/mL αCD3 and 4 μg/mL αCD28. 48 hours after activation, cells were pelleted by centrifugation and culture media was transferred to a new plate and frozen at -80°C for later analysis. The concentration of IFN-γ (430804) in the supernatant was assessed with an ELISA kit (Biolegend), following the manufacturer's instructions.

LDH-A/B enzyme activity

LDH activity was measured in the direction of reduction of pyruvate to lactate by examining the rate of NADH depletion at 340 nm at room temperature over time using an Epoch Microplate Spectrophotometer (BioTek). Briefly, 0.02 ng of recombinant human LDH (R&D Systems, LDH-A: 9158-HA-010, LDH-B: 9205-HB-050) were diluted in assay buffer (25 mM Tris, 100 mM NaCl, pH 7.5) and pre-incubated with varying concentrations of D-2HG or L-2HG for 5 minutes. The reaction was initiated by adding a substrate mixture containing NADH (0.8 mM, Sigma, N8129-100MG) and sodium pyruvate (varying concentrations) and was monitored in kinetic mode on the plate reader.

Human glioma tissue samples for MSI and CyCIF

Glioma specimens were obtained under Institutional Review Board protocols approved at Brigham and Women's Hospital (BWH) and Dana–Farber Cancer Institute with informed written consent. Each tissue specimen underwent histological evaluation for classification according to the World Health Organization classification system by board-certified neuropathologists. Specimens were flash-frozen in liquid nitrogen, sectioned to 10 μm thickness at –20°C, and thaw-mounted onto an indium tin oxide (ITO) coated glass slide. Serial sections were collected on glass microscope slides for hematoxylin and eosin (H&E) and cyclic immunofluorescence staining.

Quantification of 2HG by MSI

A tissue phantom was prepared from post-mortem human brain tissue which was homogenized and dispensed into a cryomold and frozen for calibration of the 2HG signal from tissue. A serial dilution of 2HG ranging from 0.0-20 mM was prepared in rat tail collagen type I, pipetted into a 1.5 mm channel of a 40% gelatin tissue microarray (TMA) mold, and frozen. The autopsy tissue homogenate block was cryo-sectioned to 10 μm thickness and thaw-mounted onto the same ITO slide containing the human tumor specimens. The TMA mold was then cryo-sectioned at 10 μm thickness and placed on top of the sectioned tissue homogenate. A stock solution of 2HG-d3 was prepared at 100 mM in water for use as an internal imaging standard. The 2HG-d3 stock solution (5 μL) was added to a 1,5-diaminonaphthalene hydrochloride (4.3 mg/mL) matrix solution prepared in 5 mL of 4.5/5/0.5 HPLC grade water/ethanol/1 M HCl (v/v/v). Using a TM-sprayer, the matrix was sprayed onto the whole slide to coat the matrix evenly with a four-pass cycle, flow rate (0.09 mL/min), spray nozzle velocity (1200 mm/min), spray nozzle temperature (75°C), nitrogen gas pressure (10 psi), and track spacing (2 mm). A 15 Tesla solariX FT-ICR (Bruker Daltonics, Billerica, MA) mass spectrometer operating in negative ion mode with a dual ESI/MALDI source was used for the quantitative imaging of 2HG and profiling lactate abundance from the human glioma specimens. The mass range scanned was between *m/z* 46.07-3,000 and calibrated using a tune mix solution (Agilent Technologies, Santa Clara, CA). The laser frequency was set to 1,000 Hz, and the step size was set to 100 μm with 200 laser shots per pixel. A

continuous accumulation of selected ions (CASI) window was applied with Q1 at *m/z* 150 with an isolation window of 200 *m/z*. SCiLS Lab software version (2019c premium, Bruker Daltonics, Billerica, MA) was used for ion image visualization and data analysis. Each 2HG calibration point (1.5 mm TMA spot) and tissue specimens were considered as separate ROIs and the intensity values normalized to the 2HG-d3 internal standard at *m/z* 147.0299 were exported. For each calibrant concentration 4 replicates were used. The ion intensity from each calibration ROI was plotted against the concentration to construct a linear regression model for 2HG quantitation.

Pixel-wise MSI correlation

The ion images for lactate ([M-H] *m/z* 89.0244) and 2HG ([M-H] *m/z* 147.0299) were exported to imzML using SCiLS Lab software version (2019c premium, Bruker Daltonics, Billerica, MA). The R package rMSIproc (https://github.com/prafols/rMSIproc) [54] was used for data loading, binning (2 ppm bin size) and visualization. An in-house R package was used for pixel-wise calibration of 2HG using the method described in the previous section. The correlation between lactate and 2HG in MSI was studied using an in-house R script.

Registration of MSI and CyCIF images

The CyCIF images in pyramided OME.TIFF format were imported using Open Microscopy Environment's (OME) Bio-Formats scripts for MATLAB (https://github.com/ome/bioformats). The MSI images in imzML format were imported using rMSIproc and an in-house MATLAB script. The lowest resolution pyramid level available in each CyCIF image was used for registration to minimize resolution mismatch between CyCIF-MSI image pairs. The 2HG MSI channel and Hoechst (DNA) CyCIF channels were used in the registration procedure. For each image pair, 20 to 30 pairs of fiducial markers were specified manually around the contour of the tissue. A projective transformation was used in highly similar image pairs. A piecewise linear geometric transformation was used in highly dissimilar image pairs. The MATLAB function fitgeotrans was used to obtain the transformation matrix. The 2HG and lactate MSI ion images were transformed and exported to TIFF format. The intensity scales of each image channel were adjusted to match the uint16 maximum value in the TIFF images to the maximum value for each ion channel ($2x10^7$ a.u. for the 2HG images and $2x10^6$ a.u. for the lactate images).

t-CyCIF

The t-CyCIF approach to multiplex immunofluorescence imaging has been described previously [55]. A detailed protocol can be found at Protocols.io (dx.doi.org/10.17504/protocols.io.bjiukkew). Briefly, multiplex microscopy data of primary GBM tissue specimens were collected at 20x (0.75 NA) magnification with 2x2 pixel binning using a RareCyte CyteFinder II scanning microscope. Individual image tiles had dimensions of 1280x1080 pixels and a corresponding pixel size of 0.65 μm/pixel. Four-channel (BV421, AF488, Sytox, AF647) imaging data were collected from each of three rounds of CyCIF using the following antibodies: cycle 1—Hoechst, autofluorescence (AF488), autofluorescence (AF555), autofluorescence (AF647); cycle 2—Hoechst, autofluorescence (AF488), Ki67 (Thermo Fisher, 41-5699-80) , CD8 (Thermo Fisher, 50-0008-82); cycle 3—Hoechst, CD68 (Cell Signaling, 24850S), SOX2 (Cell Signaling, 5179S), and CD45RB (Thermo Fisher, 50-9458-82). Incubation of tissue with blocking solution with secondary antibodies alone during the first cycle served to block non-specific antibody binding in the subsequent cycles. Reservation of the ultraviolet channel for nuclear counterstain (Hoechst) at each cycle allowed for cross-cycle image registration

based on cell nuclei. Raw RCPNL image files were processed into stitched, registered, and segmented multi-resolution OME-TIFF files using the MCMICRO pipeline for multiplex image processing [56]. Derived single-cell data were passed through CyLinter: a quality control filter for removing cell segmentation instances impacted by microscopy and image-processing artifacts (Baker, G. 2021. CyLinter (Version 0.0.36) [Computer software]. https://github.com/labsyspharm/cylinter). A combination of UMAP and HDBSCAN instantiated in CyLinter were used to cluster the data according to integrated antibody signal intensities.

Correlating $CD8^+$ T Cells with 2HG levels in the human glioma microenvironment

Registered MSI/CyCIF images were partitioned into equal-sized regions of tissue by applying a grid over the tissue whose x and y intervals corresponded to the pixel size of the original MSI images. For each box in the grid, the number of $CD8^+$ T cells (cluster 2 cells) was counted and the mean D-2HG pixel intensity was computed. To account for the influence of tissue density on D-2HG signal, mean 2-HG signals were divided by the total number of cells per box to yield tissue density-corrected values. Boxes with < 5 total cells, > 20% of cells affected by microscopy artifacts as determined by CyCIF analysis, or those at a tissue border were censored from the analysis to ensure data quality. Two-way, independent Welch's t-tests were used to compare tissue density-corrected D-2HG values between grid boxes with and without at least 1 $CD8^+$ T cell. Spearman's rank-order method was used to compute correlation coefficients (ρ) between tissue density-corrected D-2HG values and $CD8^+$ T cell numbers for each sample. Statistsical significance for both tests was determined at an alpha level of 0.05 ($p < 0.05$).

Low-input RNA-seq

$CD8^+$ T cells were activated in plates coated with αCD3 and αCD28 in the presence of 20 mM D-2HG, 20 mM L-2HG or left untreated. After 6 hours, cells were washed twice with PBS and the PBS was carefully removed following centrifugation. Cells were then resuspended in TCL buffer (Qiagen, 1031576) freshly supplemented with 1% BME in the proportion of 5 μL per 1000 cells. Lysates were incubated at room temperature for 5 minutes and then stored in -80°C for later analysis. RNA-seq was performed with 5 μL of the lysate using the standard ImmGen ultra-low-input RNA-seq protocol (https://www.immgen.org/img/Protocols/ImmGenULI_RNAseq_methods.pdf). Briefly, reads were aligned to the GRCm38 mouse reference genome with STAR (v2.7.3a) and gene-level quantification was performed by featureCounts (http://subread.sourceforge.net/; version 2.0.0). Raw reads counts were normalized by median of ratios method using DESeq2 package from Bioconductor (https://bioconductor.org/packages/release/bioc/html/DESeq2.html). Samples with less than 1 million uniquely mapped reads were automatically excluded from normalization to mitigate the effect of poor-quality samples on normalized counts and downstream analysis. Differential gene expression analysis was performed in R (version 4.0.0) with DESeq2 default Wald test and p-values were corrected for multiple testing using FDR/Benjamini-Hochberg method. The adjusted p-value cutoff (FDR) of <0.05 was set as a significance cut-off value. The enrichment Gene Ontology (GO) terms associated with the list of significantly differentially expressed genes (FDR <0.05) were assessed by clusterProfiler R package.

Single cell RNA sequencing analysis

We carried out analyses of annotated T cells [38] using the R package Seurat (v4.0) (https://github.com/satijalab/seurat) [57]. T cell clustering was performed using non-negative

matrix factorization (NMF) as previously described [38]. To identify differentially expressed genes between IDH-WT and IDH-mut T cells, we used t-test implemented in *FindMarkers*, and used the Bonferroni correction to perform multiple hypothesis testing on p-values. To score cells for their expression of identified genes, we calculated the signature scores using *AddModuleScore.*

Quantitative Real-Time PCR

Total RNA was isolated using Direct-zol RNA MiniPrep Kit (Genesee Scientific, 11-330). One microgram of RNA was reverse transcribed using iScript cDNA Synthesis Kit (Bio-Rad, 1708891). The qPCR was performed using PerfeCTa® SYBR® Green FastMix (QuantaBio, 101414-270) on a Roche LightCycler 480 (Roche) detection system according to the manufacturer's instruction. The following primers were used:
mGlut1 (F: GGGCATGTGCTTCCAGTATGT, R: ACGAGGAGCACCGTGAAGAT),
mHk2 (F: TGATCGCCTGCTTATTCACGG, R: AACCGCCTAGAAATCTCCAGA),
mPfk1 (F: CAGATCAGTGCCAACATAACCAA, R: CGGGATGCAGAGCTCATCA),
mLdha (F: TGTCTCCAGCAAAGACTACTGT, R: GACTGTACTTGACAATGTTGGGA),
mIFN-γ (F: TTCTTCAGCAACAGCAAGGC, R: TCAGCAGCGACTCCTTTTCC),
mIrf1 (F: GGCCGATACAAAGCAGGAGAA, R: GGAGTTCATGGCACAACGGA),
mGbp6 (F: AAGACCATGATATGATGCTGA, R: GAAAATCCATTTAAGAGAGCC),
mCxcl10 (F: CCAAGTGCTGCCGTCATTTTC, R: GGCTCGCAGGGATGATTTCAA),
mIfit3 (F: GACAGCAGTGAGAGAAGACAGAGG, R: TCTCCTTACTGATGACCATCTGATAGC),
mXaf1 (F: AGCCATGTGTCTGAGTGCAAA, GCAAAGATCACAACGGGTTTTTC),
mIigp1 (F: CAGGACATCCGCCTTAACTGT, R: AGGAAGTAAGTACCCATTAGCCA),
mGbp5 (F: CAGGACATCCGCCTTAACTGT, R: CATCGACATAAGTCAGCACCAG),
mLy6a (F: GAGGCAGCAGTTATTGTGGAT, R: CGTTGACCTTAGTACCCAGGA),
mGbp2 (F: GCAGCACCTTCATCTACAACAGC, R: CACAAAGTTAGCGGAATCGTCTACC),
mStat1(F: TCACAGTGGTTCGAGCTTCAG, R: CGAGACATCATAGGCAGCGTG),
mIgtp (F: CTCATCAGCCCGTGGTCTAAA, R: TCACCGCCTTACCAATATCTTCA),
mGbp3 (F: CTGACAGTAAATCTGGAAGCCAT, R: CCGTCCTGCAAGACGATTCA),
mTgtp2 (F: TGGGACCACTAACTTCACACC, R: GGCCAGTTGTGCATCATTTTC),
mIrgm2 (F: TCTCCGACGCTGTATTCATTCC, R: CTTCTTTCACGGCAGTCTCAAT),
mIrgm1 (F: TTTCATCAATGCACTTCGAGTCA, R: AATCCAGGTAAGTCCCACAGC),
mbActin (F: GGCTGTATTCCCCTCCATCG, R: CCAGTTGGTAACAATGCCATGT),
mGapdh (F: TTGTCTCCTGCGACTTCAACAG, R: GGTCTGGGATGGAAATTGTGAG).

Statistical analysis

Statistical analysis was performed in GraphPad Prism 9 software. Unpaired Student's t-test was used when comparing two groups. One-way analysis of variance (ANOVA) followed by Tukey-Kramer's post-hoc analysis was used when comparing three or more groups. Two-way ANOVA was used for multiple comparisons within groups. Graphs display mean ± standard deviation. P-values are denoted as *P < 0.05, **P <0.01, ***P < 0.001, ****P < 0.0001.

Table 1. Clinical and metabolic features of glioma patients samples used for MSI and CyCIF.

Diagnosis	WHO Grade	Surgery	IDH1 Status	MGMT	Case	Pyruvate (ion count)	c2HG (mM)
Diffuse Astrocytoma	2	Recurrent	R132H	Unmethylated	#01	295348.7	N/A

					#01	346490.6	N/A
					#01	279764.2	N/A
Anaplastic Astrocytoma	3	Recurrent	R132H	Unmethylated	#02	464613.9	9.19
Glioblastoma	4	Recurrent	WT	Unmethylated	#03	237869.4	N/A
					#03	220094.6	N/A
					#03	311961.9	N/A
					#03	230248.3	N/A
					#03	262390.8	N/A
					#03	364593.4	N/A
					#03	227976.9	N/A
Oligodendroglioma	3	Recurrent	R132H	Unmethylated	#04	192186.4	27.90
					#04	211060.1	51.22*
					#04	219944.7	155.71*
Astrocytoma	4	Recurrent	R132H	Methylated	#05	275612.9	188.38*
					#05	270072.8	10.34
					#05	317571.2	5.12
Glioblastoma	4	Recurrent	WT	Unmethylated	#06	223750.4	N/A
					#06	352665.1	N/A
Diffuse Glioma	N/A	N/A	R132H	N/A	#07	190251.3	2.87
					#07	282130.8	18.08
					#07	295680.5	17.98
					#07	293911.1	6.61
					#07	221516.7	2.30
Residual Oligodendroglioma	2	N/A	IDH-Mutant	1p/19q co-deleted	#08	249370.3	2.03
					#08	212681.1	5.05
Diffuse Astrocytoma	2	N/A	IDH-Mutant		#09	223833.4	3.67
					#09	81640.39	N/A
					#09	192630.3	N/A
Anaplastic Astrocytoma	3	Recurrent	R132H	Methylated	#10	264573.4	9.52
					#10	297182.6	11.42
					#10	243211.8	11.36
					#10	232207.3	18.26
					#10	212280	17.84
Anaplastic Astrocytoma	3	Recurrent	R132H	Methylated	#11	160976.5	N/A
					#11	278303.1	0.12
					#11	250703.9	0.02
Anaplastic Astrocytoma	3	Recurrent	R132H	Methylated	#12	231139.5	N/A
					#12	287784.7	16.99
					#12	307744.0	8.91

Oligodendroglioma	2	Primary	R132H	Methylated	#14	144949.9	N/A
					#14	230237.2	33.60*
					#14	239597.1	N/A
Residual Diffuse Astrocytoma	2	N/A	IDH-Mutant	N/A	#15	230996.6	70.81*
					#15	157243.6	N/A
					#15	240971.5	9.01
					#15	257925.9	53.73*
					#15	235417.5	12.11
Oligodendroglioma	2	Recurrent	R132H	Methylated	#16	235459.4	48.53*
					#16	188716.3	19.34
					#16	316835.1	89.14*
					#16	253718.3	5.49
					#16	234145.1	32.85*
					#16	225551.5	98.61*
Diffuse Astrocytoma	2	Primary	R132H	N/A	#17	261512.5	52.06*
Astrocytoma	4	Recurrent	R132H	N/A	#18	56756.66	1.25
					#18	58903.98	5.84
					#18	42286.26	N/A
					#18	14053.93	0.03
					#18	7497.919	N/A
					#18	89646.11	N/A
Astrocytoma	4	Recurrent	R132H	N/A	#19	73793.59	38.50*
					#19	61162.15	57.49*
					#19	37290.28	3.29
					#19	68269.65	51.10*
					#19	28495.6	0.17
Astrocytoma	4	Recurrent	WT	N/A	#20	2930.304	N/A
					#20	26729.67	N/A
					#20	17057.56	N/A
					#20	42720.31	N/A
					#20	43167.72	N/A
					#20	95339.29	N/A
Glioblastoma	4	Primary	WT	Unmethylated	#21	76241.08	N/A
					#21	61300.73	N/A
					#21	3276.722	N/A
Astrocytoma	4	Recurrent	R132H	Unmethylated	#22	50654.16	19.48
Glioblastoma	4	Primary	WT	Unmethylated	#23	74753.06	N/A

* Values above limit of quantification

Extended figure 1. D-2HG impairs CD8$^+$ T cell proliferation, cytotoxicity, and interferon-γ signaling in an acute and reversible fashion. (**A**) Time course of total 2HG levels in activated CD8$^+$ T cells after treatment with 20 mM D-2HG or L-2HG. Total ion count was normalized to cell number (N=3). (**B**) Viability at day 1, 3, and 6 of CD8$^+$ T cells activated with CD3/CD28 mAbs in the presence of 20 mM D-2HG, 20 mM L-2HG, or left untreated (N=3). (**C**) Induction of activation markers, CD69 and CD25, at day 3, following activation with CD3/CD28 mAbs in the presence of 20 mM D-2HG, 20 mM L-2HG, or left untreated. (**D**) Division index of CD8$^+$ T cells treated with increasing concentrations of D-2HG for 3 days (N=3). (**E**) Schematic for washout experiment to assess reversibility of proliferation phenotype. (**F**) Schematic of degranulation assay. (**G**) % degranulation of CD8$^+$ T cells treated with increasing concentrations of D-2HG (N=3). (**H**). Intracellular LAMP-1 levels in CD8$^+$ T cells treated with 20 mM D-2HG, 20 mM L-2HG, or left untreated (N=3). (**I**) % degranulation assessed by CD107a/b co-staining in CD8$^+$ T cells treated according to S1F. (**J**) % IFN-γ$^+$ (left) and IFN-γ MFI (right) of CD8$^+$ T cells treated with increasing concentrations of D-2HG (N=3). (**K**) GO enrichment analysis of most downregulated genes in CD8$^+$ T cells activated with 20 mM D-2HG relative to untreated. (**L**) Relative expression of ISGs in CD8$^+$ T cells activated with 20 mM D-2HG, 20 mM L-2HG, or left untreated (N=2-3). (**M**) Schematic of killing assay. (**N**) Nonspecific killing of B16 OVA$^-$ tumor cells by OT1 CD8$^+$ T cells that were activated in the presence of 20 mM D-2HG, 20 mM L-2HG, or left untreated (N=3). (**O**) Antigen-specific killing of B16 OVA$^+$ tumor cells by OT1 CD8$^+$ T cells that were activated in the presence of increasing concentrations of D-2HG (N=3). *P < 0.05, **P < 0.01, ***P < 0.001, ****P < 0.0001 (One-way ANOVA). Data are representative of at least two independent experiments.

Extended figure 2. D-2HG alters glycolysis in CD8$^+$ T cells. (**A**) Histone methylation western blot of CD8$^+$ T cells treated with 20 mM D-2HG, 20 mM L-2HG, or left untreated for 24 hours. (**B**) Protein levels of D-2HGDH and L-2HGDH in fully activated mouse CD8$^+$ T cells and mouse liver. (**C**) % enrichment of intracellular M+5 D-2HG after time course treatment of 20 mM $^{13}C_5$ D-2HG, showing steady state conditions (N=3). (**D**) % enrichment of intracellular M+5 L-2HG after time course treatment of 20 mM $^{13}C_5$ L-2HG, showing steady state conditions (N=3). (**E**) % enrichment of ^{13}C into 2HG and αKG after 20 mM $^{13}C_5$ D-2HG or 20 mM $^{13}C_5$ L-2HG are provided to CD8$^+$ T cells for 2 days (N=3). (**F**). Heat map showing $\log_2$ fold changes of TCA intermediates, nucleotides, and amino acids in 20 mM D-2HG- and 20 mM L-2HG-treated CD8$^+$ T cells relative to control (N=3). (**G**) Consumption and secretion map of key metabolites in the medium of cells treated with 20 mM D-2HG, 20 mM L-2HG or left untreated (N=3). (**H**) Western blot of HIF-1α stabilization in response to 20 mM D-2HG, 20 mM L-2HG, or no treatment for 24 hours. (**I**) Expression of genes involved in glucose catabolism in response 20 mM D-2HG or 20 mM L-2HG relative to the untreated control (N=3). Data are representative of at least two independent experiments.

Extended figure 3. D-2HG inhibits LDH-A activity in vitro and in CD8$^+$ T cells. (**A**) Intracellular lactate (M+3)/pyruvate (M+3) ratio of CD8$^+$ T cells treated with increasing concentrations of D-2HG (N=3). (**B**) LDH-A-mediated NADH depletion at a fixed pyruvate concentration (1 mM) and varying D-2HG concentrations (N=3). (**C**) Rate vs. substrate plot using varying concentrations of substrate and D-2HG, showing non-competitive inhibitory properties of D-2HG (N=3). (**D**) In vitro enzymatic assessment of 3 mM D-2HG, 80 μM oxamate, and 10 nM GSK2837808A on LDH-B activity (N=3). (**E**) LDH-A-mediated NADH depletion at a fixed

pyruvate concentration (1 mM) and varying L-2HG concentrations (N=3). (**F**) Rate vs. substrate plot using varying concentrations of substrate and L-2HG, showing non-competitive inhibitory properties of L-2HG (N=3). (**G**) Lineweaver-Burk plot for L-2HG. *P < 0.05, **P < 0.01, ***P < 0.001, ****P < 0.0001 (One-way ANOVA). Data are representative of at least two independent experiments.

Extended figure 4. Cytosolic NAD(H) imbalance drives mitochondrial membrane hyperpolarization in D-2HG-treated CD8$^+$ T cells. (**A**) OCR of 24-hour 20 mM D-2HG-treated CD8$^+$ T cells relative to untreated (N=10). (**B**) ECAR of 24-hour 20 mM D-2HG-treated CD8$^+$ T cells relative to untreated (N=10). (**C**) Quantification of ECAR levels in S4B. (**D**) Dose-dependent effects of D-2HG on mitochondrial membrane potential as assessed by TMRE fluorescence (N=3). (**E**) Mitochondrial membrane potential kinetics as assessed by TMRE fluorescence in response to CD8$^+$ T-cell activation in the presence or absence of 20 mM D-2HG (N=3). (**F**) Schematic for washout experiment to assess reversibility of mitochondrial membrane potential phenotype. (**G**) Mitochondrial (mt) DNA/nuclear (n) DNA ratio in response to 20 mM D-2HG or 20 mM L-2HG after 24 hours of treatment (N=3). (**H**) Protein expression of ETC subunits in response to 20 mM D-2HG treatment for 3 days (N=3). (**I**) Oxygen consumption rates of 24-hour 20 mM D-2HG-treated and untreated CD8$^+$ T cells in response to FCCP treatment (N=10). (**J**) Quantification of maximal respiration from S4I. (**K**) TMRE staining of EV-overexpressing CD8$^+$ T cells treated with 20 mM D-2HG or left untreated for 24 hours. (**L**) TMRE staining of *Lb*NOX-overexpressing CD8$^+$ T cells treated with 20 mM D-2HG or left untreated for 24 hours. **(M**) Intracellular ROS levels as assessed by CellROX staining in CD8$^+$ T cells treated with 20 mM D-2HG, 20 mM L-2HG, or control for 24 hours. (**N**) Total GSH levels in CD8$^+$ T cells treated with 20 mM D-2HG, 20 mM L-2HG, or control for 24 hours (N=3). (**O**) Total GSSG levels in CD8$^+$ T cells treated with 20 mM D-2HG, 20 mM L-2HG, or control for 24 hours (N=3). (**P**) GSH/GSSG ratio of CD8$^+$ T cells treated with 20 mM D-2HG, 20 mM L-2HG, or control for 24 hours (N=3). *P < 0.05, **P < 0.01, ***P < 0.001, ****P < 0.0001 (Student's t-test, One-way ANOVA and Two-way ANOVA). Data are representative of at least two independent experiments.

Extended figure 5. LDH inhibition recapitulates the effects of D-2HG on CD8$^+$ T-cell metabolism, proliferation, cytotoxicity, and interferon-γ signaling. (**A**) Schematic of expected incorporation of heavy carbons into glycolytic intermediates after $^{13}C_6$ glucose is provided for 24 hours and cells are simultaneously treated with control, D-2HG, or two LDH inhibitors. (**B**) Ion intensities of glycolytic intermediates and their respective ^{13}C-isotopologues after 24-hour co-treatment of $^{13}C_6$ glucose with 20 mM D-2HG, 20 mM oxamate, 10 μM GSK2837808A, or control (N=3). (**C**) Levels of secreted pyruvate isotopologues in 20 mM D-2HG-, 20 mM oxamate-, 10 μM GSK2837808A-treated, or untreated CD8$^+$ T cells (N=3). (**D**) Levels of secreted lactate isotopologues in 20 mM D-2HG-, 20 mM oxamate-, 10 μM GSK2837808A-treated, or untreated CD8$^+$ T cells (N=3). (**E**) Oxygen consumption rates of CD8$^+$ T cells treated with control, 20 mM D-2HG, 20 mM oxamate, or 10 μM GSK2837808A for 24 hours (N=10). (**F**) Extracellular acidification rates of CD8$^+$ T cells treated with control, 20 mM D-2HG, 20 mM oxamate, or 10 μM GSK2837808A for 24 hours (N=10). (**G**) Quantification of figure S5E. (**H**) mtDNA/nDNA ratio in CD8$^+$ T cells treated with 20 mM D-2HG, 20 mM oxamate, 10 μM GSK2837808A, or left untreated for 24 hours (N=3). (**I**) Viability at day 2 of CD8$^+$ T cells activated with αCD3+ αCD28 antibodies in the presence of 20 mM D-2HG, 20 mM oxamate, 10 μM GSK2837808A, or left untreated (N=3). (**J**) % degranulation assessed by LAMP-1/CD107 staining in CD8$^+$ T cells

activated in the presence of 20 mM D-2HG, 20 mM oxamate, 10 μM GSK2837808A, or left untreated. (**K**) Intracellular cytokine staining of IFN-γ in $CD8^+$ T cells activated with PMA and ionomycin in the presence of 20 mM D-2HG, 20 mM oxamate, 10 μM GSK2837808A, or left untreated. (**L**) Nonspecific killing of B16 OVA^- tumor cells by OT1 $CD8^+$ T cells that were activated in the presence of 20 mM D-2HG, 20 mM oxamate, 10 μM GSK2837808A, or left untreated (N=3). *P < 0.05, **P < 0.01, ***P < 0.001, ****P < 0.0001 (One-way ANOVA). Data are representative of at least two independent experiments.

Extended figure 6. Altered metabolic and cytotoxicity signatures in *IDH1*-mutant relative to *$IDH1^{WT}$* cancers. (**A**) Tumor weight of *$IDH1^{WT}$* and *$IDH1^{R132H}$* MC38 or B16 tumors on day 16 post inoculation (N=9-15). (**B**) Flow cytometry analysis of TILs from of *$IDH1^{WT}$* and *$IDH1^{R132H}$* MC38 or B16 tumors on day 16. Parental gate is shown below horizontal lines (N=6-10). (**C**) Quantification of percentage of $Ki67^+$ $CD4^+$ T cells in spleen and tumor of *$IDH1^{WT}$* and *$IDH1^{R132H}$* MC38 and B16 syngeneic tumor mouse models (N=6-10). (**D**) Calibration curve ranging from 0-20 mM and corresponding ion image used to determine 2HG levels in human brain tumors. (**E**) H&E stained and corresponding MSI image showing relative 2HG levels from case #19, an *$IDH1^{R132H}$* astrocytoma patient. Border between tumor and non-tumor cells is marked with a white line. (**F**) H&E stained and corresponding MSI image showing relative 2HG and lactate levels in *$IDH1^{WT}$* GBM (case #3) and *$IDH1^{R132H}$* astrocytoma (case #19) samples. (**G**) Per-pixel lactate and 2HG ion counts across all sections from case #6, an *$IDH1^{WT}$* GBM patient, and case #20, an *$IDH1^{WT}$* astrocytoma patient. Sections were annotated based on high cellularity (HC), low cellularity (LC), non-tumor (NT), and transition (T). (**H**) Per-pixel lactate and 2HG ion counts across all sections from case #18, an *$IDH1^{R132H}$* astrocytoma patient, and case #22, an *$IDH1^{R132H}$* astrocytoma patient. Sections were annotated based on high cellularity (HC), low cellularity (LC), non-tumor (NT), and transition (T). (**I**) Identification of cluster 2 cells (green scatter points) as $CD8^+$ T cells based on their morphology and co-expression of CD8α (red) and CD45RB (blue). *$IDH1^{R132H}$* astrocytoma Case #19, sample 1 shown. (**J**) H&E-stained section from Case #18, sample 3 of an *$IDH1^{R132H}$* astrocytoma showing densely cellular and even distribution of tumor cells. (**K**) Colormap of tissue density (i.e., cells per grid box) in Case #18, sample 3 (an *$IDH1^{R132H}$* astrocytoma) with the locations of $CD8^+$ T cells indicated by white scatter points. (**L**) Regression plot showing positive correlation between $CD8^+$ T cells and other cells in grid boxes from Case #18, sample 3. (**M**) H&E-stained section from Case #19, sample 1 of an *$IDH1^{R132H}$* astrocytoma showing low cellular and even distribution of tumor cells. (**N**) Colormap of tissue density (i.e., cells per grid box) in Case #19, sample 1 (an *$IDH1^{R132H}$* astrocytoma) with the locations of $CD8^+$ T cells indicated by white scatter points. (**O**) Regression plot showing positive correlation between $CD8^+$ T cells and other cells in grid boxes from Case #19, sample 1. (**P**) Left: density plot of expression of top DE upregulated genes in $CD8^+$ T-cell subpopulation in *ID^{WT}* relative to *IDH*-mutant samples. Right: density plot of expression of top DE upregulated genes in $CD4^+$ T cell subpopulation in *IDH^{WT}* relative to *IDH*-mutant samples. (**Q**) Density plot of expression of top DE upregulated genes in cytotoxicity, interferon, and Treg subclusters for $CD4^+$ T cells in *IDH^{WT}* and *IDH*-mutant samples. *P < 0.05, **P < 0.01, ***P < 0.001, ****P < 0.0001 (Student's t-test and Two-way ANOVA). Data are representative of at least two independent experiments.

References:

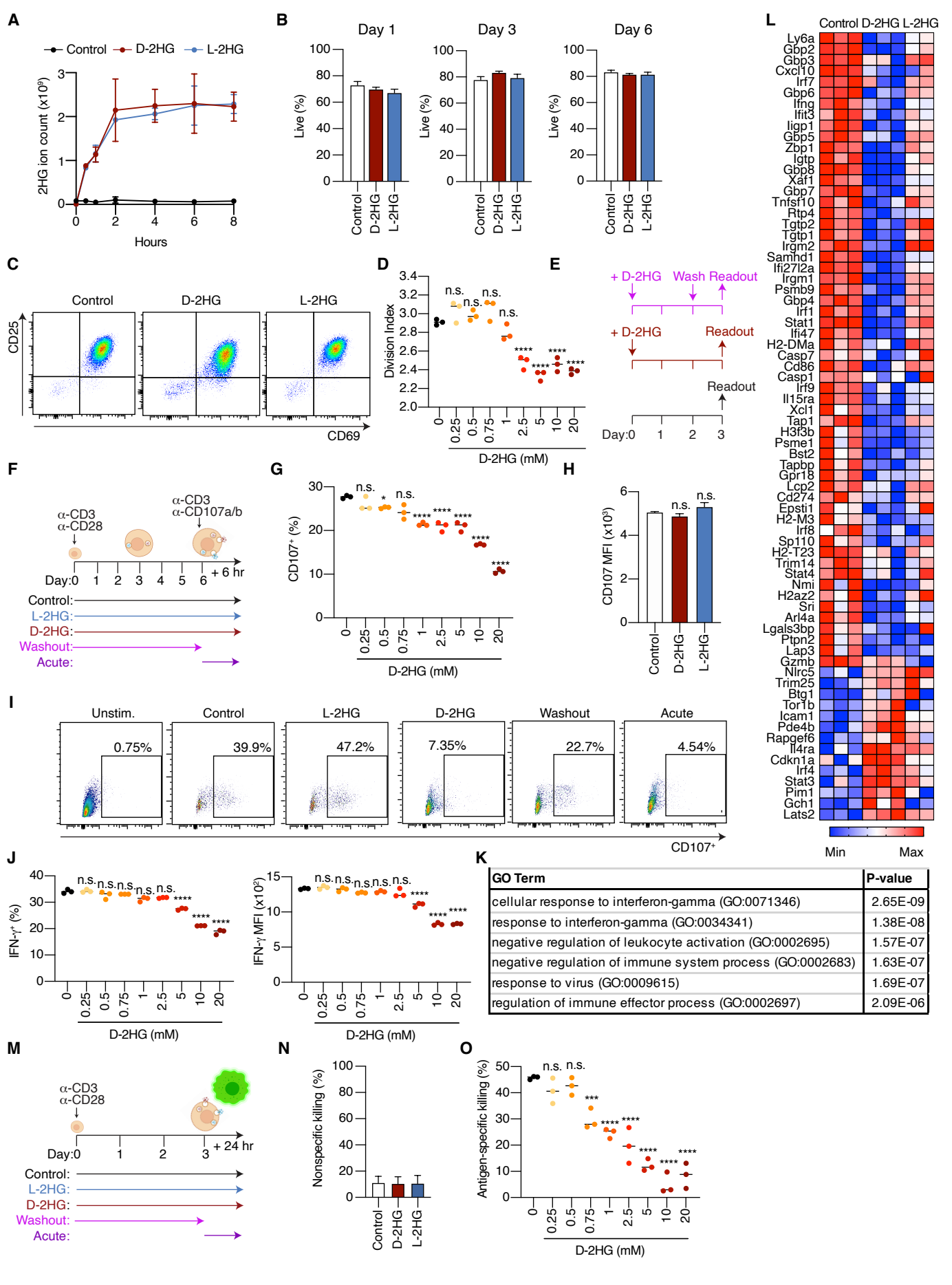
A
Control
D-2HG
L-2HG
2HG ion count (x10⁶)
Hours
B
Day 1
Day 3
Day 6
Live (%)
Control
D-2HG
L-2HG
C
Control
D-2HG
L-2HG
CD25
CD69
D
Division Index
n.s.
****
D-2HG (mM)
E
+ D-2HG
Wash
Readout
+ D-2HG
Readout
Readout
Day:0 1 2 3
F
α-CD3
α-CD28
α-CD3
α-CD107a/b
Day:0 1 2 3 4 5 6 + 6 hr
Control:
L-2HG:
D-2HG:
Washout:
Acute:
G
CD107⁺ (%)
n.s.
*
****
D-2HG (mM)
H
CD107 MFI (x10³)
n.s.
Control
D-2HG
L-2HG
L
Control D-2HG L-2HG
Ly6a
Gbp2
Gbp3
Cxcl10
Irf7
Gbp6
Ifng
Ifit3
Iigp1
Gbp5
Zbp1
Igtp
Gbp8
Xaf1
Gbp7
Tnfsf10
Rtp4
Tgtp2
Tgtp1
Irgm2
Samhd1
Ifi27l2a
Irgm1
Psmb9
Gbp4
Irf1
Stat1
Ifi47
H2-DMa
Casp7
Cd86
Casp1
Irf9
Il15ra
Xcl1
Tap1
H3f3b
Psme1
Bst2
Tapbp
Gpr18
Lcp2
Cd274
Epsti1
H2-M3
Irf8
Sp110
H2-T23
Trim14
Stat4
Nmi
H2az2
Sri
Arl4a
Lgals3bp
Ptpn2
Lap3
Gzmb
Nlrc5
Trim25
Btg1
Tor1b
Icam1
Pde4b
Rapgef6
Il4ra
Cdkn1a
Irf4
Stat3
Pim1
Gch1
Lats2
Min
Max
I
Unstim.
Control
L-2HG
D-2HG
Washout
Acute
0.75%
39.9%
47.2%
7.35%
22.7%
4.54%
CD107⁺
J
IFN-γ⁺ (%)
IFN-γ MFI (x10³)
n.s.
****
D-2HG (mM)
K
GO Term | P-value
cellular response to interferon-gamma (GO:0071346) | 2.65E-09
response to interferon-gamma (GO:0034341) | 1.38E-08
negative regulation of leukocyte activation (GO:0002695) | 1.57E-07
negative regulation of immune system process (GO:0002683) | 1.63E-07
response to virus (GO:0009615) | 1.69E-07
regulation of immune effector process (GO:0002697) | 2.09E-06
M
α-CD3
α-CD28
Day:0 1 2 3 + 24 hr
Control:
L-2HG:
D-2HG:
Washout:
Acute:
N
Nonspecific killing (%)
Control
D-2HG
L-2HG
O
Antigen-specific killing (%)
n.s.
***
****
D-2HG (mM)

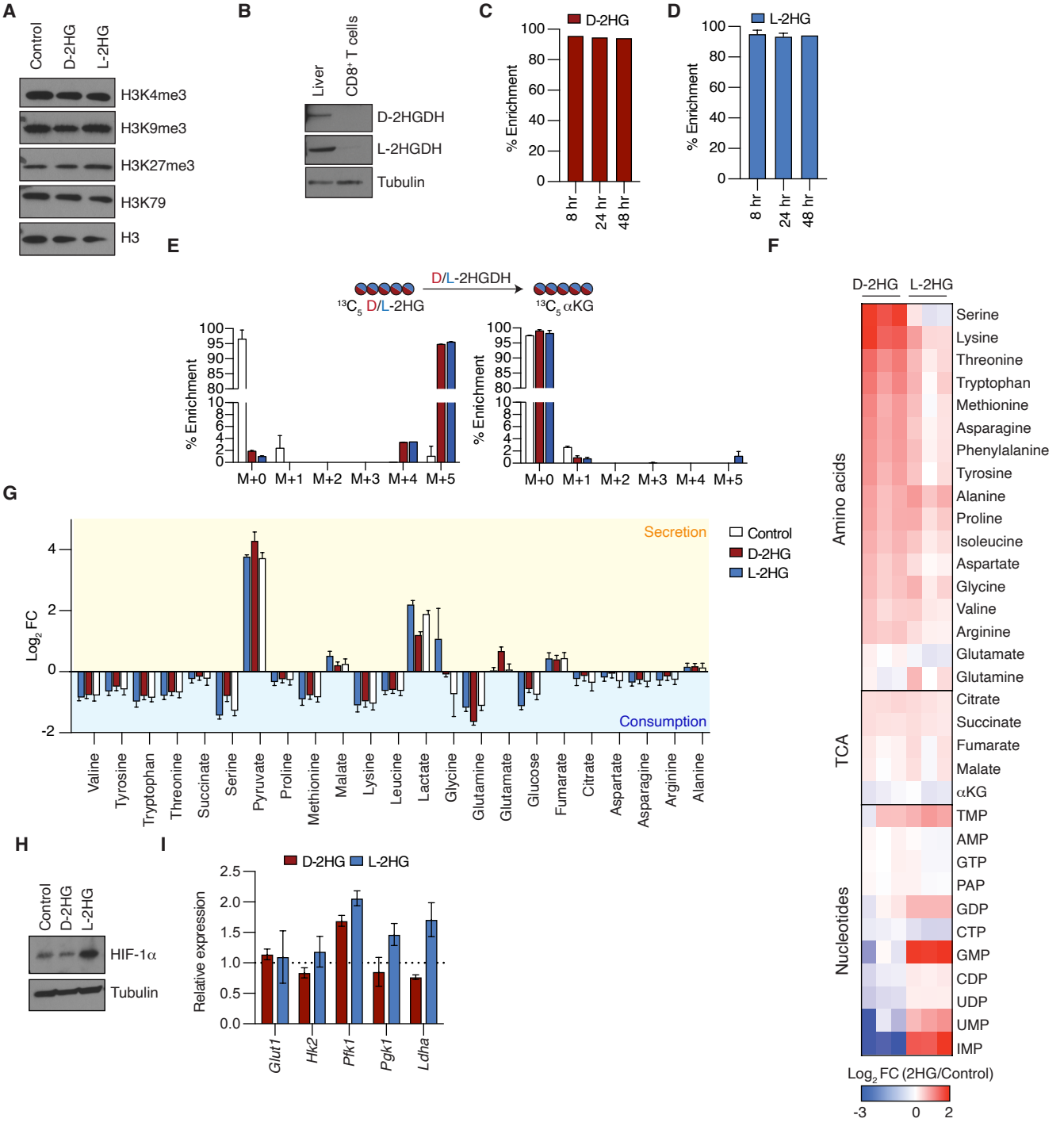
A
Control
D-2HG
L-2HG
H3K4me3
H3K9me3
H3K27me3
H3K79
H3
B
Liver
CD8+ T cells
D-2HGDH
L-2HGDH
Tubulin
C
D-2HG
% Enrichment
8 hr
24 hr
48 hr
D
L-2HG
% Enrichment
8 hr
24 hr
48 hr
E
D/L-2HGDH
13C5 D/L-2HG
13C5 αKG
% Enrichment
M+0 M+1 M+2 M+3 M+4 M+5
F
D-2HG L-2HG
Amino acids
Serine
Lysine
Threonine
Tryptophan
Methionine
Asparagine
Phenylalanine
Tyrosine
Alanine
Proline
Isoleucine
Aspartate
Glycine
Valine
Arginine
Glutamate
Glutamine
TCA
Citrate
Succinate
Fumarate
Malate
αKG
Nucleotides
TMP
AMP
GTP
PAP
GDP
CTP
GMP
CDP
UDP
UMP
IMP
Log2 FC (2HG/Control)
-3 0 2
G
Secretion
Consumption
Control
D-2HG
L-2HG
Log2 FC
Valine
Tyrosine
Tryptophan
Threonine
Succinate
Serine
Pyruvate
Proline
Methionine
Malate
Lysine
Leucine
Lactate
Glycine
Glutamine
Glutamate
Glucose
Fumarate
Citrate
Aspartate
Asparagine
Arginine
Alanine
H
Control
D-2HG
L-2HG
HIF-1α
Tubulin
I
D-2HG L-2HG
Relative expression
Glut1
Hk2
Pfk1
Pgk1
Ldha

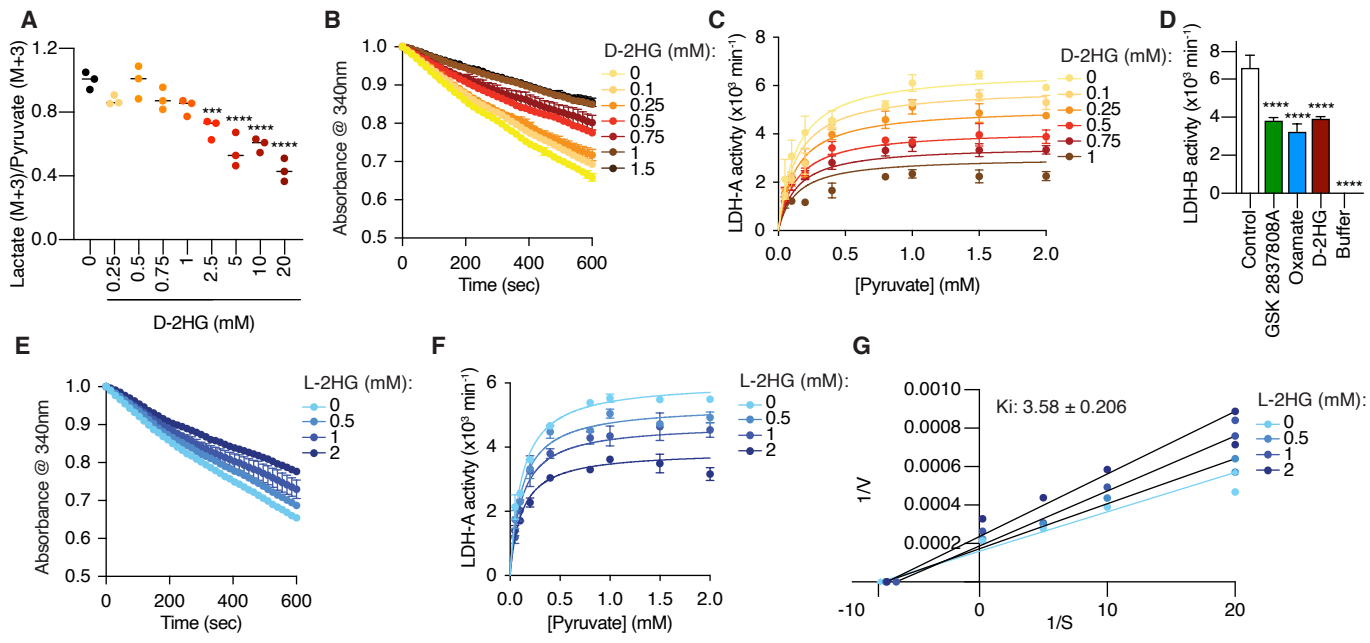
A
Lactate (M+3)/Pyruvate (M+3)
1.2
0.8
0.4
0.0
0
0.25
0.5
0.75
1
2.5
5
10
20
***
****
****
****
D-2HG (mM)
B
Absorbance @ 340nm
1.0
0.9
0.8
0.7
0.6
0.5
0
200
400
600
Time (sec)
D-2HG (mM):
0
0.1
0.25
0.5
0.75
1
1.5
C
LDH-A activity (x10³ min⁻¹)
8
6
4
2
0
0.0
0.5
1.0
1.5
2.0
[Pyruvate] (mM)
D-2HG (mM):
0
0.1
0.25
0.5
0.75
1
D
LDH-B activty (x10³ min⁻¹)
8
6
4
2
0
****
****
****
****
Control
GSK 2837808A
Oxamate
D-2HG
Buffer

E
Absorbance @ 340nm
1.0
0.9
0.8
0.7
0.6
0.5
0
200
400
600
Time (sec)
L-2HG (mM):
0
0.5
1
2
F
LDH-A activty (x10³ min⁻¹)
6
4
2
0
0.0
0.5
1.0
1.5
2.0
[Pyruvate] (mM)
L-2HG (mM):
0
0.5
1
2
G
Ki: 3.58 ± 0.206
1/V
0.0010
0.0008
0.0006
0.0004
0.0002
-10
0
10
20
1/S
L-2HG (mM):
0
0.5
1
2

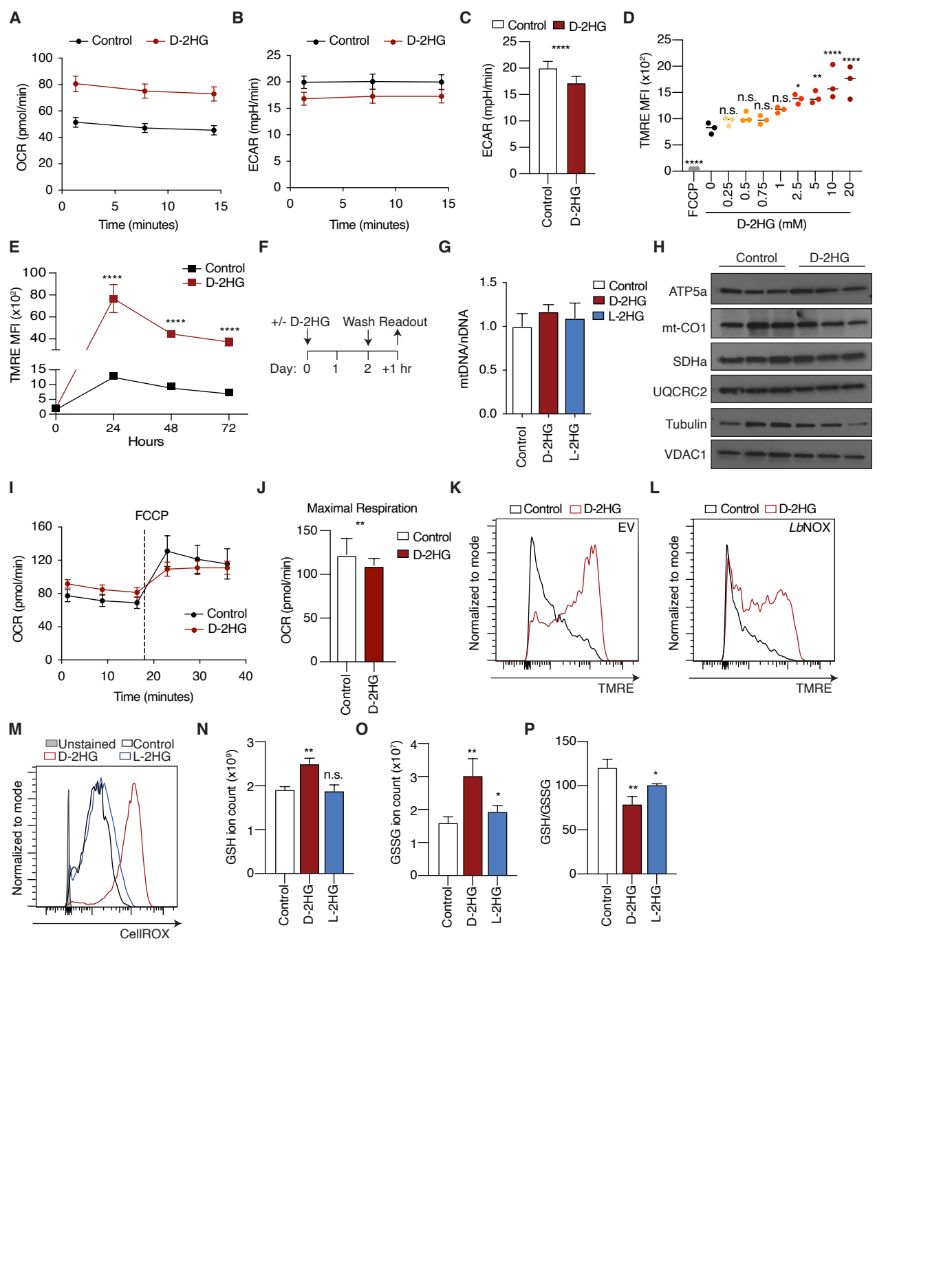
A
Control
D-2HG
OCR (pmol/min)
Time (minutes)
B
Control
D-2HG
ECAR (mpH/min)
Time (minutes)
C
Control
D-2HG
ECAR (mpH/min)
****
Control
D-2HG
D
TMRE MFI (x10³)
FCCP
0
0.25
0.5
0.75
1
2.5
5
10
20
D-2HG (mM)
n.s.
*
**
****
E
Control
D-2HG
TMRE MFI (x10³)
****
Hours
F
+/- D-2HG
Wash Readout
Day: 0 1 2 +1 hr
G
Control
D-2HG
L-2HG
mtDNA/nDNA
H
Control
D-2HG
ATP5a
mt-CO1
SDHa
UQCRC2
Tubulin
VDAC1
I
FCCP
Control
D-2HG
OCR (pmol/min)
Time (minutes)
J
Maximal Respiration
**
Control
D-2HG
OCR (pmol/min)
K
Control
D-2HG
EV
Normalized to mode
TMRE
L
Control
D-2HG
LbNOX
Normalized to mode
TMRE
M
Unstained
Control
D-2HG
L-2HG
Normalized to mode
CellROX
N
GSH ion count (x10⁹)
**
n.s.
O
GSSG ion count (x10⁷)
**
*
P
GSH/GSSG
**
*

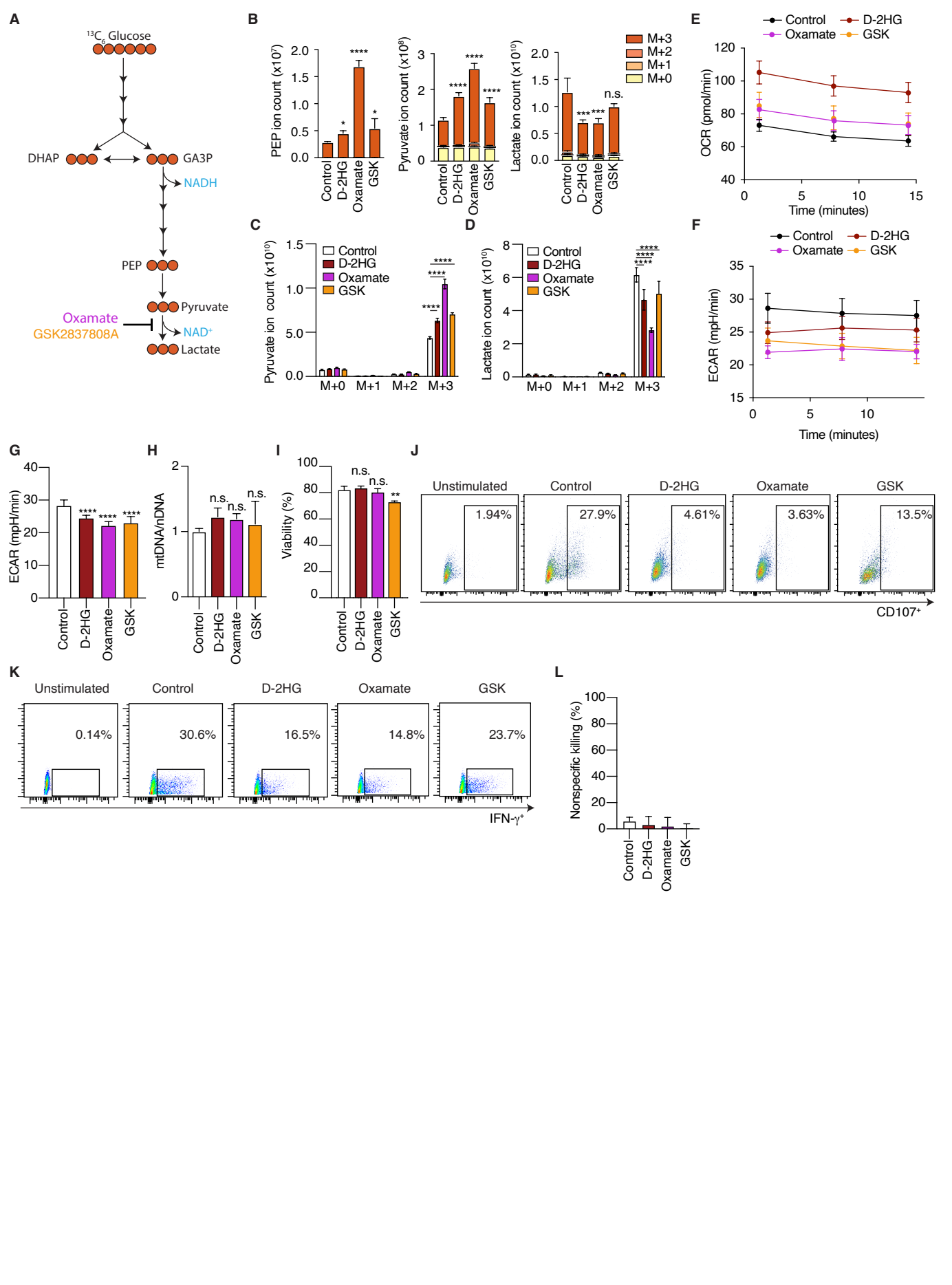
A
$^{13}C_6$ Glucose
DHAP
GA3P
NADH
PEP
Pyruvate
Oxamate
GSK2837808A
NAD+
Lactate
B
PEP ion count (x10^7)
Pyruvate ion count (x10^8)
Lactate ion count (x10^{10})
M+3
M+2
M+1
M+0
Control
D-2HG
Oxamate
GSK
n.s.
C
Pyruvate ion count (x10^{10})
D
Lactate ion count (x10^{10})
M+0
M+1
M+2
M+3
E
OCR (pmol/min)
Time (minutes)
F
ECAR (mpH/min)
Time (minutes)
G
ECAR (mpH/min)
H
mtDNA/nDNA
I
Viability (%)
J
Unstimulated
Control
D-2HG
Oxamate
GSK
1.94%
27.9%
4.61%
3.63%
13.5%
CD107+
K
0.14%
30.6%
16.5%
14.8%
23.7%
IFN-γ+
L
Nonspecific killing (%)

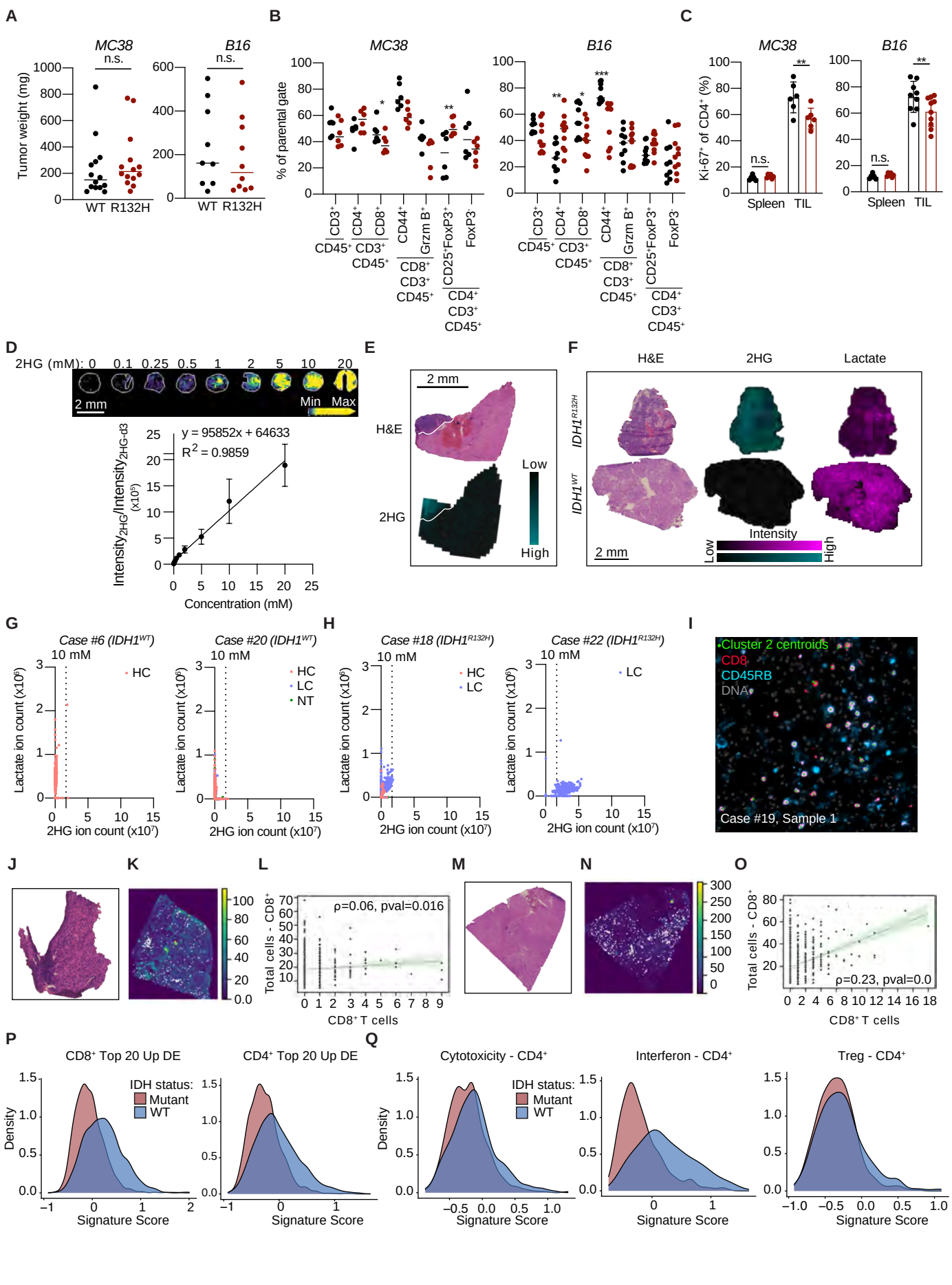
A
MC38
B16
n.s.
Tumor weight (mg)
WT R132H
B
MC38
B16
% of parental gate
CD3+ CD45+
CD4+ CD3+ CD45+
CD8+ CD3+ CD45+
CD44+ CD8+ CD3+ CD45+
Grzm B+ CD8+ CD3+ CD45+
CD25+FoxP3+ CD4+ CD3+ CD45+
FoxP3- CD4+ CD3+ CD45+
C
MC38
B16
Ki-67+ of CD4+ (%)
Spleen
TIL
D
2HG (mM): 0 0.1 0.25 0.5 1 2 5 10 20
2 mm
Min Max
y = 95852x + 64633
R2 = 0.9859
Intensity2HG/Intensity2HG-d3 (x10^5)
Concentration (mM)
E
2 mm
H&E
2HG
Low
High
F
H&E
2HG
Lactate
IDH1R132H
IDH1WT
Intensity
Low
High
2 mm
G
Case #6 (IDH1WT)
Case #20 (IDH1WT)
10 mM
HC
LC
NT
Lactate ion count (x10^6)
2HG ion count (x10^7)
H
Case #18 (IDH1R132H)
Case #22 (IDH1R132H)
I
Cluster 2 centroids
CD8
CD45RB
DNA
Case #19, Sample 1
J
K
L
ρ=0.06, pval=0.016
Total cells - CD8+
CD8+ T cells
M
N
O
ρ=0.23, pval=0.0
P
CD8+ Top 20 Up DE
CD4+ Top 20 Up DE
IDH status:
Mutant
WT
Density
Signature Score
Q
Cytotoxicity - CD4+
Interferon - CD4+
Treg - CD4+

References and Notes

1. D. G. Ryan, M. P. Murphy, C. Frezza, H. A. Prag, E. T. Chouchani, L. A. O'Neill, E. L. Mills, Coupling Krebs cycle metabolites to signalling in immunity and cancer. *Nat. Metab.* **1**, 16–33 (2019). doi:10.1038/s42255-018-0014-7 Medline

2. C. Choi, S. K. Ganji, R. J. DeBerardinis, K. J. Hatanpaa, D. Rakheja, Z. Kovacs, X.-L. Yang, T. Mashimo, J. M. Raisanen, I. Marin-Valencia, J. M. Pascual, C. J. Madden, B. E. Mickey, C. R. Malloy, R. M. Bachoo, E. A. Maher, 2-hydroxyglutarate detection by magnetic resonance spectroscopy in IDH-mutated patients with gliomas. *Nat. Med.* **18**, 624–629 (2012). doi:10.1038/nm.2682 Medline

3. L. Dang, D. W. White, S. Gross, B. D. Bennett, M. A. Bittinger, E. M. Driggers, V. R. Fantin, H. G. Jang, S. Jin, M. C. Keenan, K. M. Marks, R. M. Prins, P. S. Ward, K. E. Yen, L. M. Liau, J. D. Rabinowitz, L. C. Cantley, C. B. Thompson, M. G. Vander Heiden, S. M. Su, Cancer-associated IDH1 mutations produce 2-hydroxyglutarate. *Nature* **462**, 739–744 (2009). doi:10.1038/nature08617 Medline

4. J. A. Losman, W. G. Kaelin Jr., What a difference a hydroxyl makes: Mutant IDH, (R)-2-hydroxyglutarate, and cancer. *Genes Dev.* **27**, 836–852 (2013). doi:10.1101/gad.217406.113 Medline

5. O. C. Andronesi, G. S. Kim, E. Gerstner, T. Batchelor, A. A. Tzika, V. R. Fantin, M. G. Vander Heiden, A. G. Sorensen, Detection of 2-hydroxyglutarate in IDH-mutated glioma patients by in vivo spectral-editing and 2D correlation magnetic resonance spectroscopy. *Sci. Transl. Med.* **4**, 116ra4 (2012). doi:10.1126/scitranslmed.3002693 Medline

6. O. C. Andronesi, O. Rapalino, E. Gerstner, A. Chi, T. T. Batchelor, D. P. Cahill, A. G. Sorensen, B. R. Rosen, Detection of oncogenic IDH1 mutations using magnetic resonance spectroscopy of 2-hydroxyglutarate. *J. Clin. Invest.* **123**, 3659–3663 (2013). doi:10.1172/JCI67229 Medline

7. L. Bunse, S. Pusch, T. Bunse, F. Sahm, K. Sanghvi, M. Friedrich, D. Alansary, J. K. Sonner, E. Green, K. Deumelandt, M. Kilian, C. Neftel, S. Uhlig, T. Kessler, A. von Landenberg, A. S. Berghoff, K. Marsh, M. Steadman, D. Zhu, B. Nicolay, B. Wiestler, M. O. Breckwoldt, R. Al-Ali, S. Karcher-Bausch, M. Bozza, I. Oezen, M. Kramer, J. Meyer, A. Habel, J. Eisel, G. Poschet, M. Weller, M. Preusser, M. Nadji-Ohl, N. Thon, M. C. Burger, P. N. Harter, M. Ratliff, R. Harbottle, A. Benner, D. Schrimpf, J. Okun, C. Herold-Mende, S. Turcan, S. Kaulfuss, H. Hess-Stumpp, K. Bieback, D. P. Cahill, K. H. Plate, D. Hänggi, M. Dorsch, M. L. Suvà, B. A. Niemeyer, A. von Deimling, W. Wick, M. Platten, Suppression of antitumor T cell immunity by the oncometabolite (R)-2-hydroxyglutarate. *Nat. Med.* **24**, 1192–1203 (2018). doi:10.1038/s41591-018-0095-6 Medline

8. A. Linninger, G. A. Hartung, B. P. Liu, S. Mirkov, K. Tangen, R. V. Lukas, D. Unruh, C. D. James, J. N. Sarkaria, C. Horbinski, Modeling the diffusion of D-2-hydroxyglutarate from IDH1 mutant gliomas in the central nervous system. *Neuro Oncol.* **20**, 1197–1206 (2018). doi:10.1093/neuonc/noy051 Medline

9. R. Chowdhury, K. K. Yeoh, Y.-M. Tian, L. Hillringhaus, E. A. Bagg, N. R. Rose, I. K. H. Leung, X. S. Li, E. C. Y. Woon, M. Yang, M. A. McDonough, O. N. King, I. J. Clifton,

R. J. Klose, T. D. W. Claridge, P. J. Ratcliffe, C. J. Schofield, A. Kawamura, The oncometabolite 2-hydroxyglutarate inhibits histone lysine demethylases. *EMBO Rep.* **12**, 463–469 (2011). doi:10.1038/embor.2011.43 Medline

10. M. E. Figueroa, O. Abdel-Wahab, C. Lu, P. S. Ward, J. Patel, A. Shih, Y. Li, N. Bhagwat, A. Vasanthakumar, H. F. Fernandez, M. S. Tallman, Z. Sun, K. Wolniak, J. K. Peeters, W. Liu, S. E. Choe, V. R. Fantin, E. Paietta, B. Löwenberg, J. D. Licht, L. A. Godley, R. Delwel, P. J. M. Valk, C. B. Thompson, R. L. Levine, A. Melnick, Leukemic IDH1 and IDH2 mutations result in a hypermethylation phenotype, disrupt TET2 function, and impair hematopoietic differentiation. *Cancer Cell* **18**, 553–567 (2010). doi:10.1016/j.ccr.2010.11.015 Medline

11. S. Turcan, D. Rohle, A. Goenka, L. A. Walsh, F. Fang, E. Yilmaz, C. Campos, A. W. M. Fabius, C. Lu, P. S. Ward, C. B. Thompson, A. Kaufman, O. Guryanova, R. Levine, A. Heguy, A. Viale, L. G. T. Morris, J. T. Huse, I. K. Mellinghoff, T. A. Chan, IDH1 mutation is sufficient to establish the glioma hypermethylator phenotype. *Nature* **483**, 479–483 (2012). doi:10.1038/nature10866 Medline

12. W. Xu, H. Yang, Y. Liu, Y. Yang, P. Wang, S.-H. Kim, S. Ito, C. Yang, P. Wang, M.-T. Xiao, L. X. Liu, W. Q. Jiang, J. Liu, J. Y. Zhang, B. Wang, S. Frye, Y. Zhang, Y. H. Xu, Q. Y. Lei, K.-L. Guan, S. M. Zhao, Y. Xiong, Oncometabolite 2-hydroxyglutarate is a competitive inhibitor of α-ketoglutarate-dependent dioxygenases. *Cancer Cell* **19**, 17–30 (2011). doi:10.1016/j.ccr.2010.12.014 Medline

13. A. S. Berghoff, B. Kiesel, G. Widhalm, D. Wilhelm, O. Rajky, S. Kurscheid, P. Kresl, A. Wöhrer, C. Marosi, M. E. Hegi, M. Preusser, Correlation of immune phenotype with IDH mutation in diffuse glioma. *Neuro Oncol.* **19**, 1460–1468 (2017). doi:10.1093/neuonc/nox054 Medline

14. F. Klemm, R. R. Maas, R. L. Bowman, M. Kornete, K. Soukup, S. Nassiri, J.-P. Brouland, C. A. Iacobuzio-Donahue, C. Brennan, V. Tabar, P. H. Gutin, R. T. Daniel, M. E. Hegi, J. A. Joyce, Interrogation of the microenvironmental landscape in brain tumors reveals disease-specific alterations of immune cells. *Cell* **181**, 1643–1660.e17 (2020). doi:10.1016/j.cell.2020.05.007 Medline

15. G. Kohanbash, D. A. Carrera, S. Shrivastav, B. J. Ahn, N. Jahan, T. Mazor, Z. S. Chheda, K. M. Downey, P. B. Watchmaker, C. Beppler, R. Warta, N. A. Amankulor, C. Herold-Mende, J. F. Costello, H. Okada, Isocitrate dehydrogenase mutations suppress STAT1 and CD8+ T cell accumulation in gliomas. *J. Clin. Invest.* **127**, 1425–1437 (2017). doi:10.1172/JCI90644 Medline

16. B. Weenink, K. Draaisma, H. Z. Ooi, J. M. Kros, P. A. E. Sillevis Smitt, R. Debets, P. J. French, Low-grade glioma harbors few CD8 T cells, which is accompanied by decreased expression of chemo-attractants, not immunogenic antigens. *Sci. Rep.* **9**, 14643 (2019). doi:10.1038/s41598-019-51063-6 Medline

17. P. A. Tyrakis, A. Palazon, D. Macias, K. L. Lee, A. T. Phan, P. Veliça, J. You, G. S. Chia, J. Sim, A. Doedens, A. Abelanet, C. E. Evans, J. R. Griffiths, L. Poellinger, A. W. Goldrath, R. S. Johnson, S-2-hydroxyglutarate regulates $CD8^+$ T-lymphocyte fate. *Nature* **540**, 236–241 (2016). doi:10.1038/nature20165 Medline

18. A. M. Intlekofer, B. Wang, H. Liu, H. Shah, C. Carmona-Fontaine, A. S. Rustenburg, S. Salah, M. R. Gunner, J. D. Chodera, J. R. Cross, C. B. Thompson, L-2-Hydroxyglutarate production arises from noncanonical enzyme function at acidic pH. *Nat. Chem. Biol.* **13**, 494–500 (2017). doi:10.1038/nchembio.2307 Medline

19. S. I. Tsukumo, K. Yasutomo, Regulation of $CD8^+$ T cells and antitumor immunity by Notch signaling. *Front. Immunol.* **9**, 101 (2018). doi:10.3389/fimmu.2018.00101 Medline

20. M. Barry, R. C. Bleackley, Cytotoxic T lymphocytes: All roads lead to death. *Nat. Rev. Immunol.* **2**, 401–409 (2002). doi:10.1038/nri819 Medline

21. M. R. Betts, J. M. Brenchley, D. A. Price, S. C. De Rosa, D. C. Douek, M. Roederer, R. A. Koup, Sensitive and viable identification of antigen-specific $CD8^+$ T cells by a flow cytometric assay for degranulation. *J. Immunol. Methods* **281**, 65–78 (2003). doi:10.1016/S0022-1759(03)00265-5 Medline

22. M. D. McKenzie, N. L. Dudek, L. Mariana, M. M. W. Chong, J. A. Trapani, T. W. H. Kay, H. E. Thomas, Perforin and Fas induced by IFNgamma and TNFalpha mediate beta cell death by OT-I CTL. *Int. Immunol.* **18**, 837–846 (2006). doi:10.1093/intimm/dxl020 Medline

23. S. J. Waddell, S. J. Popper, K. H. Rubins, M. J. Griffiths, P. O. Brown, M. Levin, D. A. Relman, Dissecting interferon-induced transcriptional programs in human peripheral blood cells. *PLOS ONE* **5**, e9753 (2010). doi:10.1371/journal.pone.0009753 Medline

24. M. K. Engqvist, C. Eßer, A. Maier, M. J. Lercher, V. G. Maurino, Mitochondrial 2-hydroxyglutarate metabolism. *Mitochondrion* **19**, 275–281 (2014). doi:10.1016/j.mito.2014.02.009 Medline

25. E. A. Struys, N. M. Verhoeven, H. J. Ten Brink, W. V. Wickenhagen, K. M. Gibson, C. Jakobs, Kinetic characterization of human hydroxyacid-oxoacid transhydrogenase: Relevance to D-2-hydroxyglutaric and gamma-hydroxybutyric acidurias. *J. Inherit. Metab. Dis.* **28**, 921–930 (2005). doi:10.1007/s10545-005-0114-x Medline

26. S. P. Burr, A. S. H. Costa, G. L. Grice, R. T. Timms, I. T. Lobb, P. Freisinger, R. B. Dodd, G. Dougan, P. J. Lehner, C. Frezza, J. A. Nathan, Mitochondrial protein lipoylation and the 2-oxoglutarate dehydrogenase complex controls HIF1α stability in aerobic conditions. *Cell Metab.* **24**, 740–752 (2016). doi:10.1016/j.cmet.2016.09.015 Medline

27. S. M. Nadtochiy, X. Schafer, D. Fu, K. Nehrke, J. Munger, P. S. Brookes, Acidic pH Is a metabolic switch for 2-hydroxyglutarate generation and signaling. *J. Biol. Chem.* **291**, 20188–20197 (2016). doi:10.1074/jbc.M116.738799 Medline

28. P. Koivunen, S. Lee, C. G. Duncan, G. Lopez, G. Lu, S. Ramkissoon, J. A. Losman, P. Joensuu, U. Bergmann, S. Gross, J. Travins, S. Weiss, R. Looper, K. L. Ligon, R. G. W. Verhaak, H. Yan, W. G. Kaelin Jr., Transformation by the (R)-enantiomer of 2-hydroxyglutarate linked to EGLN activation. *Nature* **483**, 484–488 (2012). doi:10.1038/nature10898 Medline

29. A. Farhana, S. L. Lappin, "Biochemistry, lactate dehydrogenase," in StatPearls [Internet]. Treasure Island, FL: StatPearls Publishing *(*2022).

30. C. H. Chang, J. D. Curtis, L. B. Maggi Jr., B. Faubert, A. V. Villarino, D. O'Sullivan, S. C.-C. Huang, G. J. W. van der Windt, J. Blagih, J. Qiu, J. D. Weber, E. J. Pearce, R. G. Jones, E. L. Pearce, Posttranscriptional control of T cell effector function by aerobic glycolysis. *Cell* **153**, 1239–1251 (2013). doi:10.1016/j.cell.2013.05.016 Medline

31. S. Y. Lunt, M. G. Vander Heiden, Aerobic glycolysis: Meeting the metabolic requirements of cell proliferation. *Annu. Rev. Cell Dev. Biol.* **27**, 441–464 (2011). doi:10.1146/annurev-cellbio-092910-154237 Medline

32. G. J. W. van der Windt, E. L. Pearce, Metabolic switching and fuel choice during T-cell differentiation and memory development. *Immunol. Rev.* **249**, 27–42 (2012). doi:10.1111/j.1600-065X.2012.01150.x Medline

33. L. D. Zorova, V. A. Popkov, E. Y. Plotnikov, D. N. Silachev, I. B. Pevzner, S. S. Jankauskas, V. A. Babenko, S. D. Zorov, A. V. Balakireva, M. Juhaszova, S. J. Sollott, D. B. Zorov, Mitochondrial membrane potential. *Anal. Biochem.* **552**, 50–59 (2018). doi:10.1016/j.ab.2017.07.009 Medline

34. S. C. Lu, Glutathione synthesis. *Biochim. Biophys. Acta* **1830**, 3143–3153 (2013). doi:10.1016/j.bbagen.2012.09.008 Medline

35. J. B. Spinelli, M. C. Haigis, The multifaceted contributions of mitochondria to cellular metabolism. *Nat. Cell Biol.* **20**, 745–754 (2018). doi:10.1038/s41556-018-0124-1 Medline

36. D. V. Titov, V. Cracan, R. P. Goodman, J. Peng, Z. Grabarek, V. K. Mootha, Complementation of mitochondrial electron transport chain by manipulation of the NAD+/NADH ratio. *Science* **352**, 231–235 (2016). doi:10.1126/science.aad4017 Medline

37. S. E. Weinberg, N. S. Chandel, Targeting mitochondria metabolism for cancer therapy. *Nat. Chem. Biol.* **11**, 9–15 (2015). doi:10.1038/nchembio.1712 Medline

38. N. D. Mathewson, O. Ashenberg, I. Tirosh, S. Gritsch, E. M. Perez, S. Marx, L. Jerby-Arnon, R. Chanoch-Myers, T. Hara, A. R. Richman, Y. Ito, J. Pyrdol, M. Friedrich, K. Schumann, M. J. Poitras, P. C. Gokhale, L. N. Gonzalez Castro, M. E. Shore, C. M. Hebert, B. Shaw, H. L. Cahill, M. Drummond, W. Zhang, O. Olawoyin, H. Wakimoto, O. Rozenblatt-Rosen, P. K. Brastianos, X. S. Liu, P. S. Jones, D. P. Cahill, M. P. Frosch, D. N. Louis, G. J. Freeman, K. L. Ligon, A. Marson, E. A. Chiocca, D. A. Reardon, A. Regev, M. L. Suvà, K. W. Wucherpfennig, Inhibitory CD161 receptor identified in glioma-infiltrating T cells by single-cell analysis. *Cell* **184**, 1281–1298.e26 (2021). doi:10.1016/j.cell.2021.01.022 Medline

39. Y. Cao, J. C. Rathmell, A. N. Macintyre, Metabolic reprogramming towards aerobic glycolysis correlates with greater proliferative ability and resistance to metabolic inhibition in CD8 versus CD4 T cells. *PLOS ONE* **9**, e104104 (2014). doi:10.1371/journal.pone.0104104 Medline

40. C. M. Cham, G. Driessens, J. P. O'Keefe, T. F. Gajewski, Glucose deprivation inhibits multiple key gene expression events and effector functions in CD8+ T cells. *Eur. J. Immunol.* **38**, 2438–2450 (2008). doi:10.1002/eji.200838289 Medline

41. C. M. Cham, T. F. Gajewski, Glucose availability regulates IFN-gamma production and p70S6 kinase activation in CD8+ effector T cells. *J. Immunol.* **174**, 4670–4677 (2005). doi:10.4049/jimmunol.174.8.4670 Medline

42. L. F. Gemta, P. J. Siska, M. E. Nelson, X. Gao, X. Liu, J. W. Locasale, H. Yagita, C. L. Slingluff Jr., K. L. Hoehn, J. C. Rathmell, T. N. J. Bullock, Impaired enolase 1 glycolytic activity restrains effector functions of tumor-infiltrating $CD8^+$ T cells. *Sci. Immunol.* **4**, eaap9520 (2019). doi:10.1126/sciimmunol.aap9520 Medline

43. P. J. Siska, K. E. Beckermann, F. M. Mason, G. Andrejeva, A. R. Greenplate, A. B. Sendor, Y. J. Chiang, A. L. Corona, L. F. Gemta, B. G. Vincent, R. C. Wang, B. Kim, J. Hong, C. L. Chen, T. N. Bullock, J. M. Irish, W. K. Rathmell, J. C. Rathmell, Mitochondrial dysregulation and glycolytic insufficiency functionally impair CD8 T cells infiltrating human renal cell carcinoma. *JCI Insight* **2**, e93411 (2017). doi:10.1172/jci.insight.93411 Medline

44. P. C. Ho, J. D. Bihuniak, A. N. Macintyre, M. Staron, X. Liu, R. Amezquita, Y.-C. Tsui, G. Cui, G. Micevic, J. C. Perales, S. H. Kleinstein, E. D. Abel, K. L. Insogna, S. Feske, J. W. Locasale, M. W. Bosenberg, J. C. Rathmell, S. M. Kaech, Phosphoenolpyruvate is a metabolic checkpoint of anti-tumor T cell responses. *Cell* **162**, 1217–1228 (2015). doi:10.1016/j.cell.2015.08.012 Medline

45. W. J. Quinn 3rd, J. Jiao, T. TeSlaa, J. Stadanlick, Z. Wang, L. Wang, T. Akimova, A. Angelin, P. M. Schäfer, M. D. Cully, C. Perry, P. K. Kopinski, L. Guo, I. A. Blair, L. R. Ghanem, M. S. Leibowitz, W. W. Hancock, E. K. Moon, M. H. Levine, E. B. Eruslanov, D. C. Wallace, J. A. Baur, U. H. Beier, Lactate limits T cell proliferation via the NAD(H) redox state. *Cell Rep.* **33**, 108500 (2020). doi:10.1016/j.celrep.2020.108500 Medline

46. M. Peng, N. Yin, S. Chhangawala, K. Xu, C. S. Leslie, M. O. Li, Aerobic glycolysis promotes T helper 1 cell differentiation through an epigenetic mechanism. *Science* **354**, 481–484 (2016). doi:10.1126/science.aaf6284 Medline

47. J. M. Curtsinger, P. Agarwal, D. C. Lins, M. F. Mescher, Autocrine IFN-γ promotes naive CD8 T cell differentiation and synergizes with IFN-α to stimulate strong function. *J. Immunol.* **189**, 659–668 (2012). doi:10.4049/jimmunol.1102727 Medline

48. C. Chesnelong, M. M. Chaumeil, M. D. Blough, M. Al-Najjar, O. D. Stechishin, J. A. Chan, R. O. Pieper, S. M. Ronen, S. Weiss, H. A. Luchman, J. G. Cairncross, Lactate dehydrogenase A silencing in IDH mutant gliomas. *Neuro Oncol.* **16**, 686–695 (2014). doi:10.1093/neuonc/not243 Medline

49. L. J. M. Dekker, S. Wu, C. Jurriëns, D. A. N. Mustafa, F. Grevers, P. C. Burgers, P. A. E. Sillevis Smitt, J. M. Kros, T. M. Luider, Metabolic changes related to the IDH1 mutation in gliomas preserve TCA-cycle activity: An investigation at the protein level. *FASEB J.* **34**, 3646–3657 (2020). doi:10.1096/fj.201902352R Medline

50. M. M. Chaumeil, M. Radoul, C. Najac, P. Eriksson, P. Viswanath, M. D. Blough, C. Chesnelong, H. A. Luchman, J. G. Cairncross, S. M. Ronen, Hyperpolarized (13)C MR imaging detects no lactate production in mutant IDH1 gliomas: Implications for diagnosis and response monitoring. *Neuroimage Clin.* **12**, 180–189 (2016). doi:10.1016/j.nicl.2016.06.018 Medline

51. J. Balss, C. Thiede, T. Bochtler, J. G. Okun, M. Saadati, A. Benner, S. Pusch, G. Ehninger, M. Schaich, A. D. Ho, A. von Deimling, A. Krämer, C. E. Heilig, Pretreatment d-2-hydroxyglutarate serum levels negatively impact on outcome in IDH1-mutated acute myeloid leukemia. *Leukemia* **30**, 782–788 (2016). doi:10.1038/leu.2015.317 Medline

52. M. Lu, I. K. Mellinghoff, A. Diaz, J. W. Taylor, S. Choe, A. Tassinari, D. Zhu, K. Sellers, K. Le, F. Tai, I. Hassan, S. S. Pandya, L. Steelman, B. Wu, Abstract 2046: Inhibiting IDH mutations in low-grade glioma alters cellular function and the immune environment. *Cancer Res.* **80** (Supplement), 2046–2046 (2020). doi:10.1158/1538-7445.AM2020-2046

53. J. M. Drijvers, J. E. Gillis, T. Muijlwijk, T. H. Nguyen, E. F. Gaudiano, I. S. Harris, M. W. LaFleur, A. E. Ringel, C.-H. Yao, K. Kurmi, V. R. Juneja, J. D. Trombley, M. C. Haigis, A. H. Sharpe, Pharmacologic screening identifies metabolic vulnerabilities of $CD8^+$ T cells. *Cancer Immunol. Res.* **9**, 184–199 (2021). doi:10.1158/2326-6066.CIR-20-0384 Medline

54. P. Ràfols, B. Heijs, E. Del Castillo, O. Yanes, L. A. McDonnell, J. Brezmes, I. Pérez-Taboada, M. Vallejo, M. García-Altares, X. Correig, rMSIproc: An R package for mass spectrometry imaging data processing. *Bioinformatics* **36**, 3618–3619 (2020). doi:10.1093/bioinformatics/btaa142 Medline

55. J. R. Lin, B. Izar, S. Wang, C. Yapp, S. Mei, P. M. Shah, S. Santagata, P. K. Sorger, Highly multiplexed immunofluorescence imaging of human tissues and tumors using t-CyCIF and conventional optical microscopes. *eLife* **7**, 7 (2018). Medline

56. D. Schapiro, A. Sokolov, C. Yapp, Y. A. Chen, J. L. Muhlich, J. Hess, A. L. Creason, A. J. Nirmal, G. J. Baker, M. K. Nariya, J. R. Lin, Z. Maliga, C. A. Jacobson, M. W. Hodgman, J. Ruokonen, S. L. Farhi, D. Abbondanza, E. T. McKinley, D. Persson, C. Betts, S. Sivagnanam, A. Regev, J. Goecks, R. J. Coffey, L. M. Coussens, S. Santagata, P. K. Sorger, MCMICRO: A scalable, modular image-processing pipeline for multiplexed tissue imaging. *Nat. Methods* **19**, 311–315 (2022). doi:10.1038/s41592-021-01308-y Medline

57. Y. Hao, S. Hao, E. Andersen-Nissen, W. M. Mauck III, S. Zheng, A. Butler, M. J. Lee, A. J. Wilk, C. Darby, M. Zagar, P. Hoffman, M. Stoeckius, E. Papalexi, E. P. Mimitou, J. Jain, A. Srivastava, T. Stuart, L. B. Fleming, B. Yeung, A. J. Rogers, J. M. McElrath, C. A. Blish, R. Gottardo, P. Smibert, R. Satija, Integrated analysis of multimodal single-cell data. bioRxiv 2020.10.12.335331 [Preprint] (2020); https://doi.org/10.1101/2020.10.12.335331.